

Figure 8.4 Transient responses at 10MHz with THD<1%

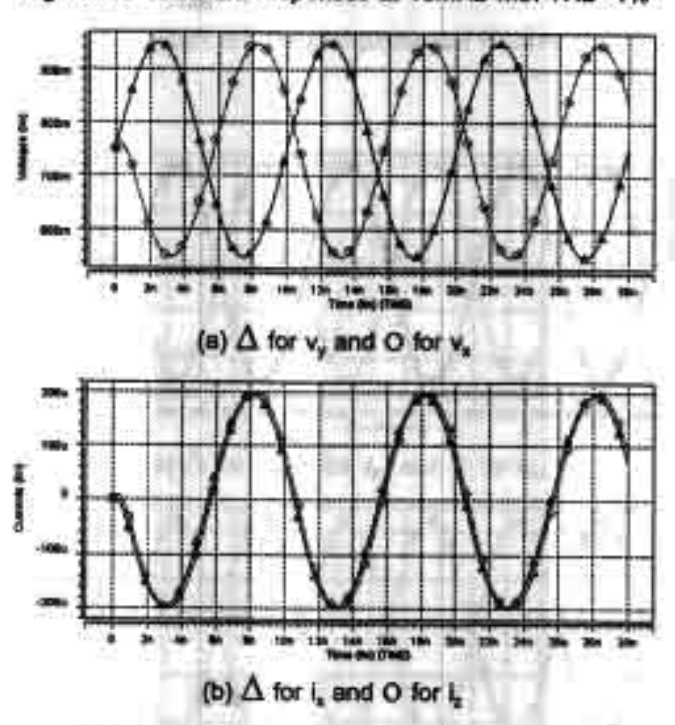


Figure 8.5 Transient responses at 100MHz with THD<1%

In many current conveyor applications, there is a need to have both polarities of output current  $i_z$  or multiple outputs  $i_z$ , and  $i_z$ . In some conventional CCII, this facility is usually performed using additional current mirrors to copy and invert polarity of the output current  $i_z$ . However non-ideal characteristics of current mirror always introduce some tracking error between the current  $i_z$ , and  $i_z$ . In the similar way on this topology, we can not straightforwardly cascade additional inverters at the output Z terminal in order to make an inverted-direction current  $i_z$ , since there is usually an excess phase shift that causing an unperfected tracking between the currents  $i_z$ , and  $i_z$ . In this case, we demonstrate a parallel connected ICCII+s as shown Fig.8.6. Fig.8.7 (a) shows a perfected tracking of the voltage signal at terminals  $v_{y1}$ ,  $v_{x1}$  and  $v_{x2}$ . The perfected tracking in both magnitude and out of phase of  $i_{z*}$  and  $i_z$  are shown in Fig.8.7 (b) confirming a high precision property of this ICCII+.

connected PMOSs producing the large resistors are always in reverse bias because the voltage at the floating-gate is small as a result of the negative feedback. With  $\pm 0.75 \text{V}$  supply, the circuit can handle signal swing as large as  $\pm 500 \mu\text{A}$  amplitude through X and Z terminals and  $\pm 500 \text{mV}$  at Y and X terminals while the THD is maintained to less then 1%. The circuit is designed to operate up to 100MHz signal frequency.

## 9. A HIGH SPEED LOW INPUT CURRENT LOW VOLTAGE CMOS CURRENT COMPARATOR

In the last decade, current-mode circuits [39, 43, 54] have drawn lots of interest for modern integrated circuits and sensory systems. This is due to their attractive features such as high speed, wide dynamic ranges and low voltage operation, all of which are mainly due to the fact that all node voltages swing are very low. In analogue and mixed signal processing, the current comparator is also one of the key elements. The circuit is not purely in a current-mode operation since although the input signal is current the output signal is digital logics or rail to rail voltage signal. Obviously there is a requirement to transform the input current to a large voltage signal. Thus to design a high speed current comparator, one has to take care of the voltage swing carefully since it directly determines the propagation delay. Conventionally, most reported current comparators [60-63] are based on the concept shown as a block diagram in Fig.9.1 (a), where the input current signal is converted to the voltage Vin and V1 by the transimpedance stage comprising inverter amplifier A1 and voltage buffer A2. The resulting voltage V<sub>t</sub> is then amplified by the latter high gain inverter amplifiers A<sub>3</sub> to produce output logic voltage. There exist parasitic capacitors at all nodes, ideally for high speed comparators, the signal swing at V1 should be maintained as small as possible and situated exactly around the inverter threshold voltage of the inverter A<sub>3</sub>. However, the reported works were relating to improve the lowest input current acquiring ability by arranging a proper biasing to turn on the MOSFETs of the buffer A2 all the time. Most of them utilized diode connected MOSFETs as a level shifter to create V<sub>GS</sub> of the buffer MOSFETs. It is seen that although the transimpedance stage is formed in a negative feedback loop a much larger loop gain has not been exploited to keep the signal Vin and Vi as low as possible. Moreover with a larger loop gain, the input impedance at node V<sub>in</sub> could be much lower and receive a much smaller input current in the pico Amps range. The so called dead zone which is the smallest input current range to which comparators are insensitive is then minimized. However, a drawback of having the small voltage swing at Vt is that the gain of the latter inverter amplifier must be necessarily high with hence a higher power consumption. Obviously, there is a conflict that if a speed as a result of a small voltage swing of the transesistance stage is desired, a very high gain of the latter inverter amplifier will be necessary to provide the rail to rail output swing. In this paper, we propose an idea based on Fig.9.1 (b), where a much higher loop gain is emphasized to gain speed and then trade power to the latter

high gain inverter amplifier. The circuit utilizes only CMOS inverters and is suitable for a low V<sub>DD</sub> operation.

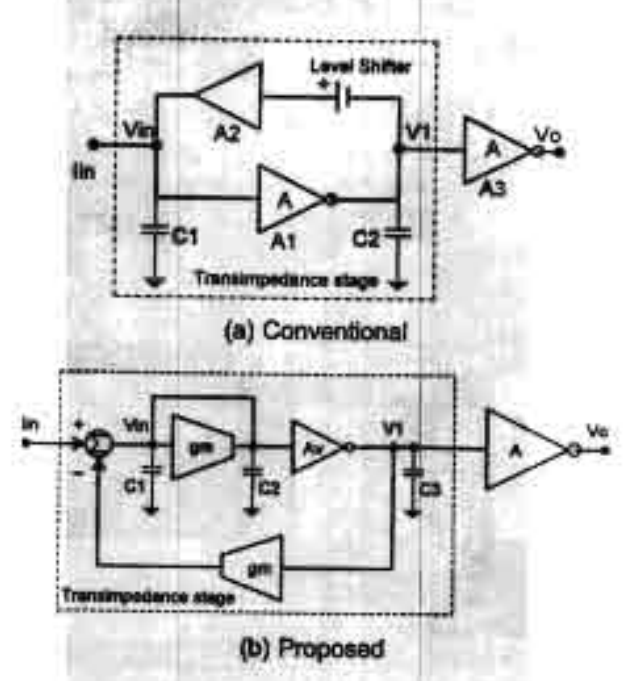


Figure 9.1 Current comparator concepts

## 9.1 THE PROPOSED CIRCUIT

As discussed above, we concentrate on a high speed or smallest average propagation delays and low input current acquiring capability or smallest dead zone. In this work, we trade off power for the required speed by maintaining the lowest voltage swing of the transimpedance stage and then providing high power to build up the latter high gain stage using inverter amplifiers. We then focus on the two separated circuit blocks as follows.

## 9.1.1 TRANSIMPEDANCE STAGE

The transimpedance stage, shown as the dashed block in Fig.9.2, plays the most important role in determining the speed of the comparator. It is seen that the whole stage is formed in a negative feedback loop by observing the polarities of output voltages and currents of each inverter. At as a shorted input-output transconductance amplifier or inverter is basically an equivalent grounded resistor with the value of 1/gm. At and At are two high voltage gain amplifiers constructed from two cascaded inverters. Since there are two high impedance nodes in the loop RC frequency compensation is necessary to make the circuit stable. Capacitor C is set to 0.1pF while the resistor R is set to 1.6k Ohms. Note that the C and R could be made from a parasitic capacitor and a triode MOSFET respectively. The transconductance amplifier At is used to provide

negative feedback current to the input node, All amplifiers A<sub>1</sub> to A<sub>4</sub> are CMOS inverters designed with the same dimensions which are 2.1um/0.25um and 7um/0.25um for W/L of NMOS and PMOS respectively.

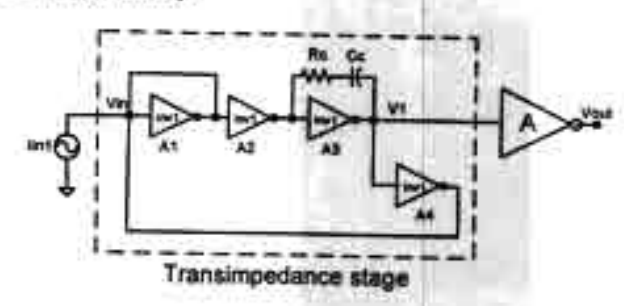


Figure 9.2 Transimpedance stage

Constructed in the feedback loop, the input resistance at node V<sub>in</sub> can be derived as.

$$R_{in} = \frac{1}{gm_T \left(1 + A_{in}^2\right)}$$
 (9.1)

where  $gm_T$  is an equivalent transconductance of  $A_t$  and and  $A_{vo}$  is a voltage gain of the amplifier  $A_2$  and  $A_3$ . Note that all inverters have the same transconductance and voltage gain because they have the same dimensions. It is seen that the input resistance  $R_n$  is very small which results in a minimum voltage swing at node  $V_{in}$  and also the same value of  $V_1$  at the output of  $A_3$ . Fig.9.3 shows an open loop gain and phase of the feedback current to the input current. It is seen that dc gain of 56dB, GBW of 906MHz and PM of  $45^{\circ}$  are achieved in the open loop transconductance stage. With this specification, we have enough loop gain to suppress signals for the lowest voltage swings at  $V_{in}$  and  $V_1$  as shown in Fig.9.4. The negative feedback also stabilizes the common-mode voltage at all nodes to  $V_{00}/2$  which is set by the node  $V_{in}$ . This property is crucial for assuring that the signal swing is very small and also situated right at the center of the gate threshold voltage of the latter inverter of the gain stage.

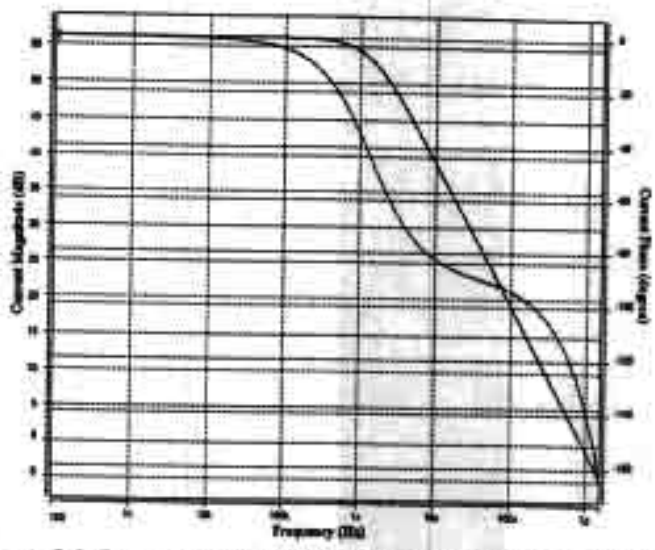


Figure 9.3 Open-loop responses of the transconductance stage

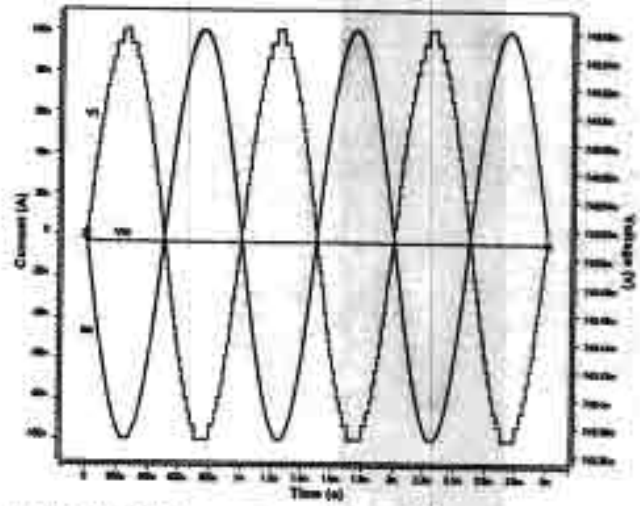


Figure 9.4 Voltage swings at Vie and Vi vs. input current

#### 9.1.2 GAIN STAGES

We have now a very small voltage swing V<sub>1</sub> at the input of A<sub>5</sub> of the gain stage. The main aim in designing this part is to construct high voltage gain to produce rail to rail output logic. Based on the use of the same dimension inverters, the high gain stage can be constructed in a modular fashion as shown in Fig.9.5. INV1 has the same dimension as those in the transconductance stage. INV2 has smaller dimensions than those of INV1 by half, i.e. 1um/0.25um and 3.5um/0.25um for W/L of NMOS and PMOS respectively. The modules could be placed in parallel for higher gain. For A<sub>5</sub>, there are six INV1s connected in parallel, where each INV1 possesses an output current equal to the inverter does not deteriorate the speed much because each inverter has a very small propagation delay which is less than 1ns. So as discussed earlier the major contributor to the delay is the transimpedance stage.

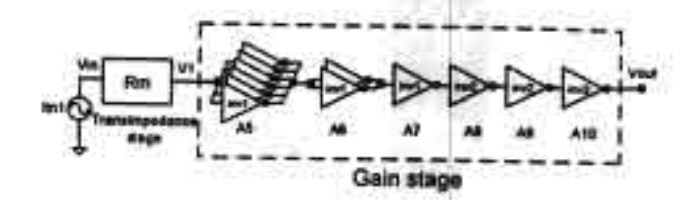


Figure 9.5 Gain stage

#### 9.2 SIMULATION RESULTS

The proposed current comparator has been designed on a 0.25um TSMC CMOS process and tested with various power supplies and input current amplitudes. On HSPICE and with V<sub>DO</sub> set to 1.5V, the comparator responses of three input current amplitudes of 1uA, 100nA and 100pA are shown in Fig.9.6 where the average propagation delays are 1.95ns, 3.6ns and 10.7ns respectively. Performances vs the input current amplitudes at 1.5V V<sub>00</sub> such as average propagation delay, static power and power delay product (PDP) are shown in Fig.9.7. It is seen that the lowest input current amplitude is at ±50pA thanks to the small input resistance as a result of the negative feedback with high loop gain. The average propagation delay is inversely proportional to the input current amplitudes since the voltage swing at the output of the transconductance stage is small. With small input current amplitudes, the static power also increases because all node voltages are around the common-mode value or V<sub>DD</sub>/2 where most MOSFETs of the inverters are fully turned on. Propagation delays at various V<sub>DD</sub> and input signal amplitudes are shown in Fig.9.8. Performance comparisons among many reported circuits are listed in Table 9.1. It is seen that the power is higher than those from some earlier designs because the scaling down of the V<sub>DD</sub> normally degrades some properties of the inverter such as average drain current, voltage gain and propagation delay. Thus more power has to be pumped into the circuits in order to achieve the required speed and rail to rail output voltage swing.

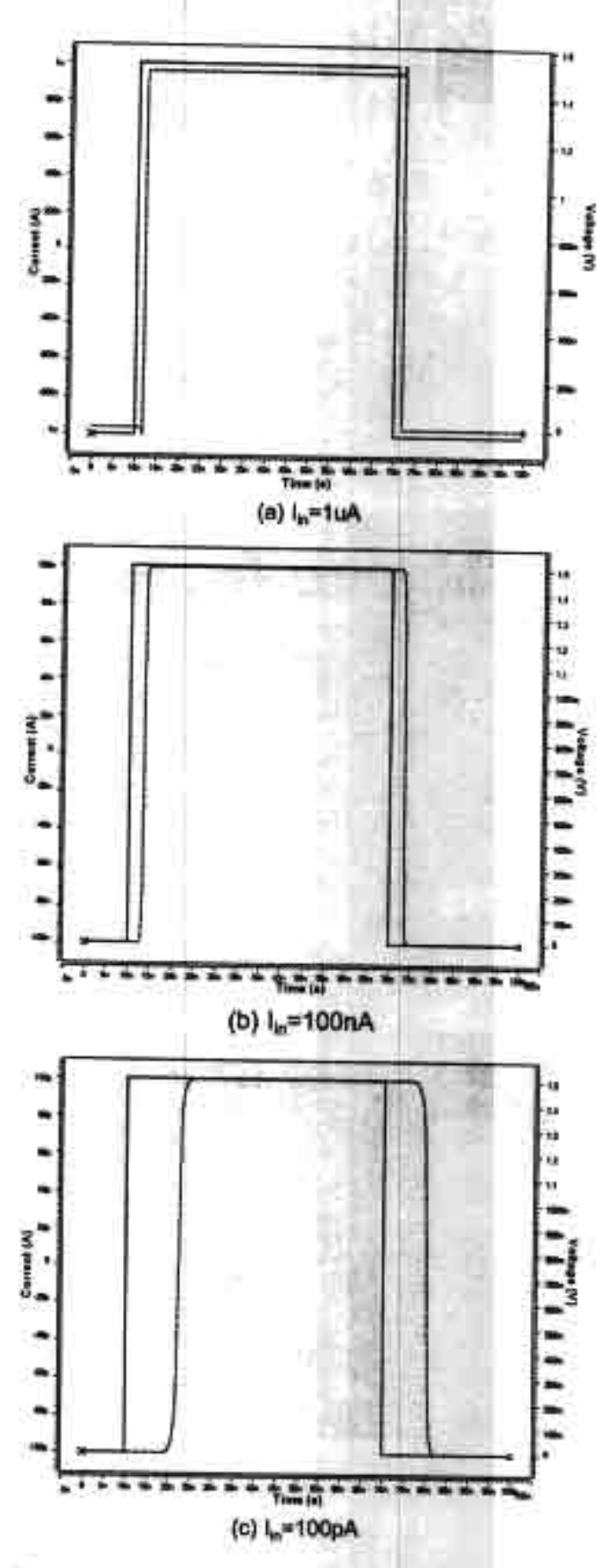


Figure 9.6 Transient Response of Vour vs. In at 1.5V Voo

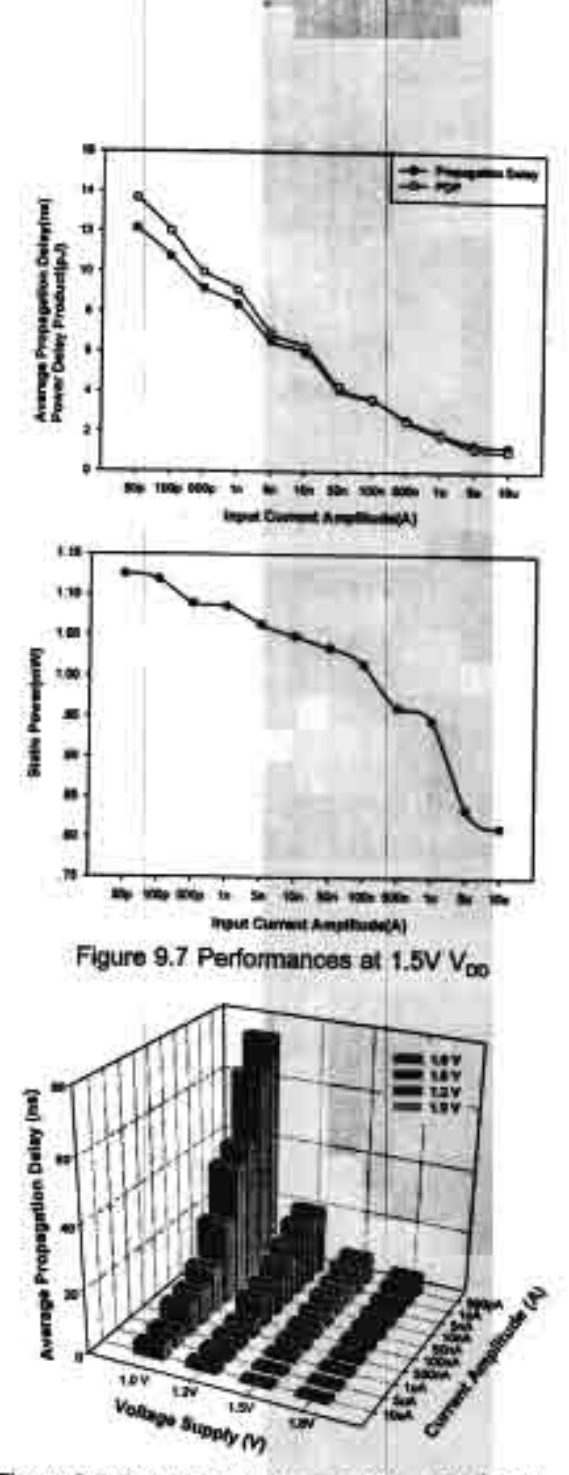


Figure 9.8 Propagation delays at V<sub>pg</sub> 1.0-1.8 Volts

A new high speed low input current low voltage current comparator has been demonstrated on a 0.25um TSMC CMOS process. Based on the concept of a high speed current-mode technique, we exploit a negative feedback scheme around the transimpedance stage with an emphasis on a very large loop-gain to produce a very small transformed voltage swing which is situated at the center of the gate threshold voltage of the latter stage. This will ensure the fastest response time. The same dimension inverters are used in all amplifier stages. They are fast and simple and suitable for low voltage operation. There is no extra biasing circuit and stacked

transistor, thus the same design can be applied with various  $V_{00}$  - le there is no need to readjust the design.

		T	able 9.1 Perfor	mance com	partsons	N .		
	Traff [60]	Tang [61]	Ravezzi[62]	Min [64]	Lin [63]		roposed circ	oult
Year	1992	1994	1997	1966	2000	2002	2002	2002
Power Supply (V)	5	8	5	3	3	1.5	1.0	1.8
Process (µm)	2	1.6	2.5	0.35	0.35	0.25	0.25	0.25
Minimum Input Current Amplitude (nA)	10	10	100	10		0.05	0.05	0.5
Propagation delay	±1µA/	±0.1µA/ 11ne	±0.1µW	±0.1µW	±0.1µA/ 2.8ms	±0.1µA/ 3,5na	±0.1µA/	±0.1µA/
Power consumption (mW) (at 0.1µA)	0.390	14.	M	0.45	0.58	1.01	0.022	2.73
PDP (pJ)	NA .	NA .	NA	3.15	1.4	3.848	0.32	7.25

## 10. CONCLUSION

A floating-gate MOSFET or FGMOS on a standard double-poly CMOS offers various new useful functions which can be used to create many novel circuits such as low voltage low power circuits, analogue computational circuits and etc. This report gives a review of FGMOS such as the principle properties, functional characteristics and modeling for simulation tools. FGMOS device is basically a multiple-input device of which the main properties can be very useful for analog and digital computational circuits. It has unique and attractive characteristics of which the most important properties to be applied in this research and report are as follows: 1) As a multiple-input gate device, the voltage appears at the floating gate is a linear summation of its input voltage at all input terminals. This characteristic makes the device suitable for multiple signal computation. 2) The effective threshold voltage (V<sub>th</sub>) seen at the input gate is tunable. These two phenomena are very attractive to analog designers. The first feature of the multiple-input gates allows analog designers to design a novel or to adapt many existing circuits to work with more complexity function without adding power consumption, while the second feature allows FGMOS devices to be operated at a very low the supply voltage as a result of the threshold voltage tunability. Both low voltage and low power operations are the most important requirement for biomedical applications. In this research, several analog signal processing building blocks have been proposed. They are very useful to various applications in biomedical systems such as biologically inspired circuits, electronic cochlea, silicon retina and analogue neural networks.

A Hysteresis Tunable Voltage Comparator using FGMOS is already proposed. The circuit is essentially exploiting FGMOS devices in the positive feedback scheme to create the hysteresis. Based on the tunability of the FGMOS, the current ratio of I<sub>D10</sub>/I<sub>D3</sub> and I<sub>D11</sub>/I<sub>D4</sub> corresponding to the amount of feedback current is used to tune the hysteresis effectively. An experiment of the back-gate tuning of M3 and M4 has also been investigated with a result showing that the range of V<sub>TRP</sub>, and V<sub>TRP</sub>, are not as wide as those offered by the circuit employing FGMOS. Also, the back-gate biasing always experiences an amount of leakage current because the bulk terminal is not fully isolated as in the case of poly1 and poly2 gates. The proposed idea can be implemented on any standard double-poly CMOS processes. The work has been performed on AMI 1.2μm CMOS process available through MOSIS. All the simulation

results confirm well the functionality. Performance optimizing will be placed as future works. Following the design of the Hysteresis Tunable Voltage Comparator, a non-clocked 8-bits digital comparator is also presented. It essentially manipulates the proposed analog voltage comparator to realize the new digital circuit in which the signal is internally processed in an analogue fashion. The proposed idea can be implemented on any standard double-poly CMOS and be useful to mixed signal and computational applications. All the simulation results confirm well the functionality.

As an application of a multiple input voltage comparator, designs of a single-chip low-voltage high-efficiency Class-D Power Amplifier for portable devices has been proposed. The amplifier has a very simple architecture that makes it easier to be integrated with other circuit blocks on a system level. By virtue of the high efficiency of Class-D architecture coupled with the low voltage operation provided by the use of floating-gate MOSFET hysteresis comparator, this amplifier is suitable for portable devices with battery operations. It exhibits high distortion at low input signal due to the small changing of the input signal compared to the ripple at the output. The efficiency of this circuit is 95% at 0.88Watt with a 2.8V power supply.

In this research, a novel approach in exploitation of CMOS inverter in a negative feedback form is presented. Normally, the CMOS Inverter has only one input terminal which is not convenience to be used in a negative feedback form. However, the negative feedback can be performed successfully via an assistance of the floating-gate additive analog inverter. A new low voltage wide swing current amplifier is then proposed. It can receive a signal swing as large as ±200µLA amplitude while a THD of about 1% is still maintained. The circuits can totally be realized in the class AB thanks to the use of CMOS inverters and the available additive analog inverter cells using floating-gate MOSFETs. The circuit is called a current amplifier instead of opamp due to the lack of CMRR capability, which will be part of our future works. Based on the same concept of designing CMOS inverter circuits in a negative feedback form, a low voltage wide swing inverting second generation CMOS current conveyor of which the design focuses on the use of CMOS inverters and the negative feedback to enhance conveying precisions, signal linearity and low output resistance property at the terminal X. The circuit is totally realized in class AB thanks to the use of CMOS inverters and the available floating-gate MOSFET additive analog inverter cell which facilitates the negative feedback channel to the normal CMOS inverter. With the programming approach of pseudo or quasi floating-gate MOSFET, DC offset of the floating-gate

inverter can be effectively controlled to Vdd/2 and the complicated initial charge programming schemes could be avoided. The diode connected PMOSs producing the large resistors are always in reverse bias because the voltage at the floating-gate is small as a result of the negative feedback. With ±0.75V supply, the circuit can handle signal swing as large as ±500µA amplitude through X and Z terminals and ±500mV at Y and X terminals while the THD is maintained to less then 1%. The circuit is designed to operate up to 100MHz signal frequency.

A new high speed low input current low voltage current comparator has also been proposed and demonstrated on a 0.25um TSMC CMOS process. Based on the concept of a high speed current-mode technique, a negative feedback scheme has been exploited around the transimpedance stage with an emphasis on a very large loop-gain to produce a very small transformed voltage swing which is situated at the center of the gate threshold voltage of the latter stage. This will ensure the fastest response time. The same dimension inverters are used in all amplifier stages. They are fast and simple and suitable for low voltage operation. There is no extra biasing circuit and stacked transistor, thus the same design can be applied with various V<sub>DD</sub> - ie there is no need to readjust the design.

This research works have been leading the way to exploit the floating-gate MOSFET device in various low voltage low power applications based on the fundamental concepts of analog signal processing and current mode circuit designs. All proposed analog building blocks are useful for micro power system designs and integrations. The first attempt in using the CMOS inverter in negative feedback form has been pointed out and should be exploited further for future works.

## 11. REFERENCES

- [1] Liming Yin, S.H.K. Embabi, E. Sanchez-Sinencio, "A floating-gate MOSFET D/A converter," in Proc. ISCAS '97, 1997, vol. 1, pp. 409-412.
- [2] R. R. Harrison, J. A. Bragg, P. Hasler, B. A. Minch, S. P. Deweerth, "A CMOS programmable analog memory-cell array using floating-gate circuits," IEEE Trans. Analog and Digital Signal Processing, vol. 48 Issue 1, pp. 4-11, Jan 2001.
- [3] E. O. Rodriguez, A. Yufera, A. Rueda, "A gm-C floating-gate MOS integrator" in Proc. ISCAS 2000, 2000, vol. 4, pp.153 -156.
- [4] K. Yang, A. G. Andreou, "Multiple Input floating-gate MOS differential amplifiers and applications for analog computation," in Proc of the 36th Midwest Symposium on Circuits and Systems 1993, 1993, vol. 2, pp. 1212-1216.
- [5] Y. Berg, S. Aunet, O. Ness, H. Gundersen, M. Hovin, "Extreme low-voltage floating-gate CMOS transconductance amplifier," in Proc. ISCAS 2001, 2001, vol. 1, pp. 37-40.
- [6] R. R. Harrison, "Floating gate current mirror for gain correction in CMOS translinear circuits", in Proc. ISCAS '99,1999, vol. 2, pp. 404-407.
- [7] T. Shibata, M. Konda, Y. Yamashita, T. Nakai, T. Ohmi, "Neuron-MOS-based association hardware for real-time event recognition," in Proc. Microelectronics for Neural Networks, 1996, pp. 94-101.
- [8] H.R. Mehrvarz, C. Y. Kwok, "A novel multi-input floating-gate MOS four-quadrant analog multiplier," IEEE Journal of Solid-State Circuits, vol. 31, Issue: 8, Aug. 1996 pp. 1123-1131.
- [9] Y. Berg, O. Naess, M. Hovin, "Ultralow-voltage floating-gate analog multiplier with tunable linearity," in Proc. ISCAS 2000, 2000, vol. 4, pp. 245-248.
- [10] D. Kahng, S. M. Sze, "A Floating-Gate and its Application to Memory Devices," The Bell System Technical Journal, vol. 46, no. 4, pp. 1288-1295, 1967.
- [11] M. Holler, S. Tam, H. Castro, R. Benson, "An electrically trainable artificial neural network (ETANN) with 10240 'floating gate' synapses," International Joint Conference on Neural Networks, 1989, vol. 2, pp.191-196.
- [12] P. Hasier, B. A. Minch, C. Diorio, "Floating-gate devices: they are not just for digital memories any more," in Proc. ISCAS '99, 1999, vol. 2, pp. 388-391.
- [13] A. Thomsen, M. A. Brooke, "Low control voltage programming of floating gate MOSFETs and applications," IEEE Trans Circuit and systems, vol. 41, no. 6, pp. 443-452, June 1994

- [14] T. Shibata, T. Ohmi, "A functional MOS translator featuring gate-level weighted sum and threshold operations," IEEE Trans Electron Devices, vol. 39, Issue: 6, pp. 1444-1455, June 1992.
- [15] C. Mead, Analog VLSI and Neural Systems, Reading, MA: Addison-Wesley, 1989.
- [16] T. Inoue, H. Nakane, Y. Fukuju, "A low-voltage fully-differential current-mode analog CMOS integrator using floating-gate MOSFETs," in Proc. ISCAS 2000, 2000, vol. 4, pp. 145-148 vol.4
- [17] J. Ramirez-Angulo, R. G. Carvajal, J. Tombs, A. Torralba, "A.Low-voltage CMOS op-amp with rail-to-rail input and output signal swing for continuous-time signal processing using multiple-input floating-gate transistors," IEEE Trans Circuits and Systems II: Analog and Digital Signal Processing, vol. 48, Issue: 1, pp. 111-116, Jan 2001.
- [18] B. A. Minch, P. Hasler, C. Diorio, "Multiple-Input translinear element networks," in Proc. ISCAS '98, 1998, vol. 1, pp. 88 -91.
- [19] F. Osamu, A. Yoshihito, "A Floating-Gate Analog Memory Device for Neural Networks," IEEE Trans. Electron Devices, vol. 40, no. 11, Nov. 1993.
- [20] P. Hafliger, C. Rasche, "Floating gate analog memory for parameter and variable storage in a learning silicon neuron," in Proc. ISCAS '99, 1999, vol. 2, pp. 416-419.
- [21] K. Yang, A. G. Andreou, "Subthreshold analysis of floating-gate MOSFET's," in Proc. The Tenth Biennial University/Government/Industry Microelectronics Symposium, 1993, pp. 141-144
- [22] J. Ramirez-Angulo, G. Gonzalez-Altamirano, S. C. Choi, "Modeling Multiple-input Floating-gate transistors for analog signal processing," in Proc.ISCAS'97, 1997, vol. 3, pp. 2020-2023.
- [23] K. Yang; A. G. Andreou, "The multiple input floating gate MOS differential amplifier; an analog computational building-block," in Proc. ISCAS '94, 1994, vol. 5, pp. 37-40.
- [24] B. A. Minch, P. Hasler, C. Diorio, "Multiple-input translinear element networks," in Proc. ISCAS '98, 1998, vol. 1, pp. 88-91.]
- [25] Y. Berg, D. T. Wisland, T. S. Lande, S. Mikkelsen, "Ultra low-voltage digital floating-gate UVMOS (FGUVMOS) circuits," in Proc. ISCAS '98,1998,vol. 2, pp. 37-40.

- [26] J. Ramirez-Angulo, S. C. Choi, G. Gonzale-Altamimo, "Low-Voltage Circuit Building Blocks Using Multiple-Input Floating-Gate Transistors," IEEE Transcircuits and system: fundamental theory and applications, vol.42, no.11, Nov 1995
- [27] Y. Berg, O. Naess, M. Hovin, "Ultra low-voltage floating-gate transconductance amplifier with tunable gain and linearity," in Proc. ISCAS 2000, 2000, vol. 3 pp. 343-346.
- [28] P. Klein, K. Hoffmann, O. Kowarik, "An EEPROM compact circuit model," in Proc. Custom Integrated Circuits Conference 1996, 1996, pp. 325-328.
- [29] G. V. Steenwijk, K. Hoen, H. Wallinga, "A nonvolatile analog programmable voltage source using the VIPMOS EEPROM structure," IEEE J. Solid-State Circuits, vol. 28, no. 7, pp. 784-788, July 1993.
- [30] C. K. Sin, A. Ktamer, V. Hu, R. R.Chu, P. K. Ko, "EEPROM as an analog device, with particular application in neural," IEEE Trans. Electron devices, vol. 39 no. 6, pp. 1410-1419.
- [31] C. Hu, "Lucky Electron Model of Channel Hot Electron Emission," International Electron Device Meeting Technical Digest, pp. 22-5, 1979.
- [32] R. H. Fowler, L. Nordheim, "Electron Emission in Intense Electric Fields," in Proc. The Royal Society of London, 1928, vol. A119, pp. 81-173
- [33] "IEEE standard definitions and characterization of floating gate semiconductor arrays," IEEE Std 1005-1998, 9 Feb. 1999
- [34] P. E. Allen, D. R. Hoberg, CMOS Analog Circuit Design. NY: Oxford University press, pp. 323-362
- [35] D. L. Schilling, C. Belove, Electronic Circuits Discrete And Integrated, 3<sup>rd</sup> edition, McGraw-Hill, 1989
- [36] B. Duncan, High Performance Audio Amplifiers, Newnes, 1996
- [37] L. Kitjalak, P. Pawawongsak, "DSP Application for RWDM Inverters", The 22nd Electrical Engineering Conference, Bangkok, 1999, pp. 541-544
- [38] Choi et al, "A design of a 10-W single-chip class D Audio amplifier with very high efficiency using CMOS technology," IEEE Trans. Consumer electronics, vol. 45, no.3, Aug 1999
- [39] C. Toumazou, F.J. Lidgey, D. Haigh, "Analogue IC Design: The current-mode Approach", Peregrinus, UK, 1990.

- [40] G. Palmisano, G. Palumbo, S. Pennisi, "CMOS Current Amplifiers", Kluwer Academic Publishers, 1999.
- [41] E. Abou-Allam, E.I. El-Masry, "A 200 MHz Steered current operational amplifier in 1.2-µm CMOS Technology", IEEE J. Solid-State Circuits, vol. 32, 1997, pp. 245-249.
- [42] S. Jun, D.M. Kim, "Fully differential current operational amplifier", Elec. Lett., vol. 34, 1998, pp. 62-63.
- [43] G. Palmisano, S. Pennisi, "Low-Voltage continuous-time CMOS current amplifier with dynamic biasing", Proc. ISCAS2001, pp. I-312-I-315.
- [44] R.H. Zele, S. Lee, D.J. Alistot, "A high gain current-mode operational amplifier", Proc. ISCAS92, pp. 2852-2855.
- [45] T. Kaulberg, "A CMOS current-mode operational amplifier", IEEE J. Solid-State Circuits, vol. 28, 1993, pp. 849-852.
- [46] E. Bruun, "A high-speed CMOS current-mode op-amp for very low supply voltage operation", Proc. ISCAS94, pp.509-512.
- [47] E. Abou-Allam, E.I. El-Masry, "High CMRR CMOS current operational amplifier", Elec. Lett., vol. 30, 1994, pp. 1042-1043.
- [48] T. Shibata, T. Ohmi, "A Functional MOS Transistor Featuring Gate-Level Weighted Sum and Threshold Operations", IEEE Trans. Elec. Devices, vol. 39, 1992, pp. 1444-1455.
- [49] M.A. Ibrahim, H. Kuntman, "A CMOS realization of inverting second generation current conveyor", Proc. 2002, NORDIC Signal Processing Symposium, 2002.
- [50] M.T. Abdelma'Atti, N.A. Tasadduq, "New current-mode controlled filters using the controlled conveyor", Int. J. of Electronics, Vol.85, No.4, 1998, pp.483-488.
- [51] U. Yodprasit, "High-precision CMOS current conveyor", Electronics Letters, Vol. 36, No. 7, March 2000, pp.609-810.
- [52] B. Maundy, I. Finvers, P. Aronhime, "A low voltage CMOS current conveyor for active filter design", Proc. MWSCAS-1998, August, 1998.
- [53] A. J. Lopez-Martin, J. Ramirez-Angulo, R. G. Carvajal, "Low-voltage low-power wideband CMOS current conveyors based on the flipped voltage follower", Proc. ISCAS2003, pp.I-801-804.
- [54] K. Moolpho, J. Ngarmnil, K. Nundhasri, "A low-voltage wide-swing FGMOS current amplifier", Proc. ISCAS2002, May, 2002.

- [55] T. Shibata, T. Ohmi, "A Functional MOS Transistor Featuring Gate-Level Weighted Sum and Threshold Operations", IEEE Trans. Elec. Devices, vol. 39, 1992, pp. 1444-1455.
- [56] O. Naess, Espen A. Olsen, Y. Berg, T. S. Lande, "A low voltage second order biquad using pseudo floating-gate transistors", Proc. ISCAS2003, pp. I-125-128.
- [57] J. Ramirez-Angulo, A. J. Lopez-Martin, R. G. Carvajal, C. Lackey, "Low-voltage closed-loop amplifier circuits based on quasi-floating gate transistors", Proc. ISCAS2003, pp.I-813-816.
- [58] J. Ramirez-Angulo, C. Urquidi, R. G. Carvajal, A.Torralba, "Sub-voit supply analog circuits based on quasi-floating gate transistors", Proc. ISCAS2003, pp.1-781-784.
- [59] I.A. Awad, A.M. Soliman, "Inverting second generation current conveyors: the missing building blocks, CMOS realizations and applications", Int. J. Electronics, Vol. 86, pp.413-432, 1999.
- [60] H. Traff, "Novel approacch to high speed CMOS current comparators", Electronics Letters, Vol.28, No.3, pp.310-312, 1992.
- [61] A.T.K. Tang and C. Toumazou, "High performance CMOS current comparator", Electronics Letters, Vol.30, No.1, pp.5-6, 1994.
- [62] L.Ravezzi, D.Stoppaa and G.F. Dalta Betta, "Simple high-speed CMOS current comparator", Electronics Letters, Vol.33, No.22, pp.1829-1830, 1997.
- [63] H. Lin, J.H. Huang and S.C. Wong, "A simple high-speed low current comparator", IEEE Trans. Circuit Syst., pp.713-716, 2000.
- [64] B.M. Min and S.W. Kim, "High performance CMOS current comparator using resistive feedback network", Electronics Letters, Vol.34, No.22, pp.2074-2076, 1998.

# ผลลัพธ์จากโครงการวิจัยที่ได้รับทุนจาก สกว.

การนำผลงานวิจัยไปใช้ประโยชน์ในเชิงวิชาการโดยมี การผลิตนักศึกษาระดับบัณฑิตศึกษาสองคน คือ

- [1] นาย กฤษณพงศ์ นันทศรี ปริญญาวิศวกรรมศาสตรมหาบัณฑิต สาชาวิชาวิศวกรรมไฟฟ้า สาชาย่อยวิศวกรรมอิเล็กทรอนิกส์ สำเร็จปีการศึกษา พ.ศ. 2544
- [2] นางสาว กรณีการ์ มูลโพธ์ กำลังจัดทำวิทยานิพนธ์ระดับปริญญาดุษฎีบัณฑิด สาขาวิชา วิศวกรรมไฟฟ้า สาขาย่อยวิศวกรรมอิเล็กทรอนิกส์ การนำเสนอผลงานในที่ประชุมวิชาการระดับนานาชาติ
- K. Nandhasri, J. Ngarmnil, "Designs of Analog and Digital Comparators with FGMOS", 2001 IEEE International Symposium on Circuits and Systems (ISCAS2001), Sydney, May, 2001.
- [2] K. Moolpho, J. Ngarmnil, K. Nandhasri, "A low-voltage wide-swing FGMOS current amplifier", 2002 IEEE International Symposium on Circuits and Systems (ISCAS2002), Phoenix, May, 2002.
- [3] K. Nandhasri, J. Ngarmnil, K. Moolpho, "A 2.8V RWDM BTL Class-D Amplifier using an FGMOS Comparator", 2002 IEEE International Symposium on Circuits and Systems (ISCAS2002), Phoenix, May, 2002.
- [4] J. Ngarmnil, K. Nandhasri, K. Moolpho, "Floating-gate MOSFETs Analog Circuit Building Blocks: Design perspective", 2002 IEEE International Symposium on Communication and Information Technology, Thailand, October, 2002. (Invited paper)
- [5] K. Moolpho, J. Ngarmnil, S. Sitjongsataporn, "A high speed low input current low voltage CMOS current comparator", 2003 IEEE International Symposium on Circuits and Systems (ISCAS2003), Bangkok, May, 2003.
- [6] J. Ngarmnil, S. Ruengrungson and K. Nandhasri, 'A 100MHz ±0.75V FLOATING-GATE MOSFET CURRENT CONVEYOR', 2003 IEEE Midwest Symposium on Circuits and Systems (MWSCAS2003), Cairo, December, 2003.

## ภาคผนวก

[1] K. Nandhasri, J. Ngarmnii, "Designs of Analog and Digital Comparators with FGMOS", 2001 IEEE International Symposium on Circuits and Systems (ISCAS2001), Sydney, May, 2001.

## DESIGNS OF ANALOG AND DIGITAL COMPARATORS WITH FGMOS

K. Nandhasri and J. Ngarmuil

Electronic Engineering Department, Mahanakom University of Technology, Bangkok, Thailand 10530 Email: jitkasame@ee.mut.ac.th

#### ABSTRACT

Designs of snalog and digital comparators are presented in this paper. We exploit the threshold voltage operation characteristic of floating-gate MOSPETs to produce a hysteresis-tunable analog voltage comparator. Consequently, the proposed analog comparator circuit is developed to a digital comparator using replacement of floating-gate MOSPETs for the input devices of which the drain currents are linear sums of the weighted multiple-input voltages which are then applied as binary bits. Simulation results on 1.2µm CMOS are demonstrated.

#### 1. INTRODUCTION

Recently, many applications of floating-gate (PGMOS) devices in analog circuits have been reported [1]-[10]. However, in electronic systems, the voltage comparator is also a very widely used circuit element found in many applications. This paper presents designs for analog and digital comparators based on an explosiation of the FGMOS. A hysteresis-tunable analog comparator is constructed with an electronically tunable positive feedback factor obtained by threshold voltage tuning of the embedded FGMOSs. Recently, a design for an 8-bit digital comparator working in an analog feshion was proposed [1]. The circuit was intended for less complexity, size and improved speed. This paper also presents an alternative design of an 8-bit digital comparator featuring arithmetic functions of A>B and A≥B. The circuit essentially manipulates the proposed analog voltage comparator to produce a new digital circuit in which the signal is internally processed in an analog fashion. As a consequence, the new comparator is achieved by virtue of the analog technique.

## 2. FGMOS BASIC PRINCIPLES

Figure 1. The FGMOS symbol

An FCMOS is an ordinary MOSFET except that the conventional gate on polyl is floated. The equivalent structure, shows in Figure 1, comprises a floating gate on polyl and input gates  $(G_1,...,G_n)$  built on polyl which are coupled to the polyl gate by the capacitors  $(C_1,...,C_n)$  between polyl and polyl. With UV illumination, zero initial charge on the floating-gate can be assumed. In such a case, the drain current of the PGMOS can be written as

$$I_{b} = \frac{1}{2} \mu C_{ac} \frac{W}{L} \left[ (k_{1} V_{G1} + ... + k_{s} V_{Gn}) - V_{s} - V_{TN} \right]^{2}$$
 (1)

$$I_D = \frac{1}{2} \mu C_{ac} \frac{W}{L} [(k_1 V_{G1} - V_S) - (V_{D1} - k_2 V_{G2})]^2$$
 (2)

where  $k_1,...,k_n$  are  $C_P/C_T,...,C_P/C_T$  respectively and  $C_T$  is the total capacitance of the floating gate. The drain current is essentially a linear sum of all the input voltages weighted by the capacitive coupling ratios. Furthermore, equation (1) can be rearranged to (2) in order to show the threshold operation when only two input gates are assumed. It is seen that  $V_{OI}$  can be utilized as a signal port while  $V_{OI}$  is used to tune the effective threshold voltage. These two features are exploited in this work.

## 3. HYSTERESIS ANALOG COMPARATOR

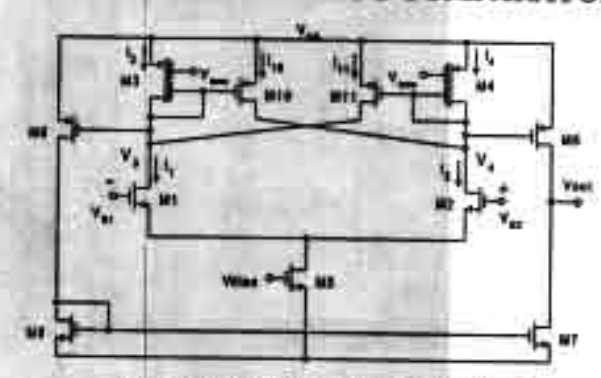


Figure 2. The Hysteresis Analog Comparator

A simple hysteresis analog comparator is well discussed in [11] and shown in altered form in Figure 2 where M3 and M4 are FGMQSs. The hysteresis involves two positive feedback paths provided by M10 and M11. The positive feedback occurs only when the current ratios of I<sub>10</sub>I<sub>3</sub> and I<sub>10</sub>I<sub>4</sub> are both greater than unity. If these ratios increase fighter, the feedback current will also increase resulting in wider positive and negative trip point voltages (V<sub>TEP</sub>, and V<sub>TEP</sub>.). Hence the hysteresis can be controlled. An equation can be developed for V<sub>TEP</sub>, from the condition that whenever the circuit operates in the hysteresis loop, I<sub>2</sub> always equals I<sub>10</sub>. Similarly for V<sub>TEP</sub>, with I<sub>2</sub> set equal to I<sub>31</sub>. We have

$$V_{TRP-} = \sqrt{\frac{2I_3}{\beta_1}} \frac{\sqrt{I_{10}/I_3} - 1}{\sqrt{1 + I_{10}/I_3}}$$

$$V_{TRP-} = \sqrt{\frac{2I_4}{\beta_1}} \frac{\sqrt{I_{11}/I_4} - 1}{\sqrt{1 + I_{11}/I_4}}$$
(3)

where  $\beta_1$  is the  $\mu C_m W/L$  for M1 which is identical to that of M2. Thus, from (2), by virtue of the FGMOSs, the ratios of  $I_{Div}/I_{D1}$  and  $I_{D1v}/I_{D1}$  can be tuned electronically by the voltage  $V_{max}$  at the input gates  $V_{C2}$  of M3 and M4. Hence  $V_{TRV}$  and  $V_{TRV}$  can be naned orthogonally if the tuning voltage at the input gates of M3 and M4

are different. M3 and M4 are designed with the areas of the two input gates equal to 10.8×22.8µm² while the conventional gate areas are set to 13.2×2.4 µm², the same as those of M10 and M11. The circuit was simulated on HSPICE using 1.2µm AMI CMOS with assistance from the FGMOS macro model in [1] and supply voltage set to 5.0V. Figure 3 shows V<sub>TRP</sub>, and V<sub>TRP</sub>, vs. V<sub>mm</sub> varied in the range of 2.5-5.0V.

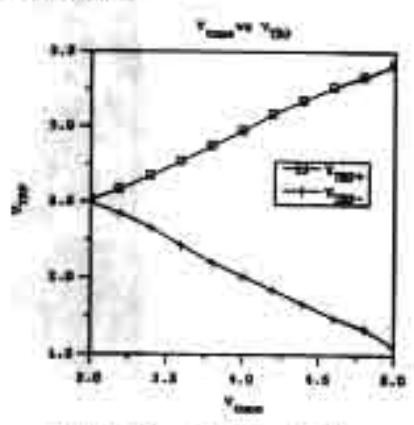


Figure 3. Vynn- and Vynn- vs. V

Time-domain simulation was also performed to express the performance of the comparator in a noisy environment. The circuit was tested with a noise-modulated signal of which the noise amplitude set to 0.4V<sub>pess</sub> while V<sub>less</sub> was set to 3.8V. Simulation results are shown in comparison with those from a non-hysteresis comparator in Figure 4.

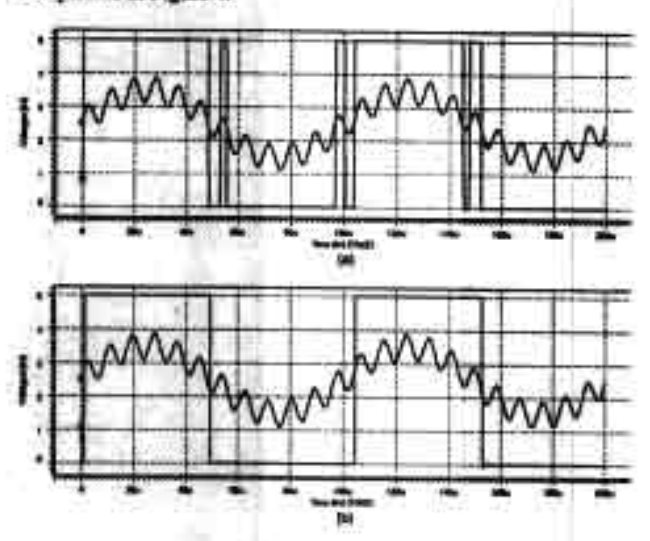


Figure 4. Comparison of results from (a) non-hysteresis and (b) hysteresis comparator

#### 4. 4-BITs DIGITAL COMPARATOR

Based on the proposed opamp-based analog comparator, a new 4bits digital comparator can also be realized by employing PGMOSs as the input devices. These 4-bit digital comparators are proposed separately as non-bysteresis and hysteresis types. Both circuits are further used for designing an 8-bit digital comparator that will be discussed in the next section. The non-hysteresis digital comparator is shown in Figure 5. It is seen that FGMOSs are employed as the input devices in order to exploit the drain current, which was written in (1) as a linear sum of the weighted multiple-input voltages that are basically binary bits of digital input data. Binary bits of '1' and '0' correspond to the voltage V<sub>Al</sub> and 0V at the input nodes respectively. The circuit is digital at the input and output but internally works at an analog circuit.

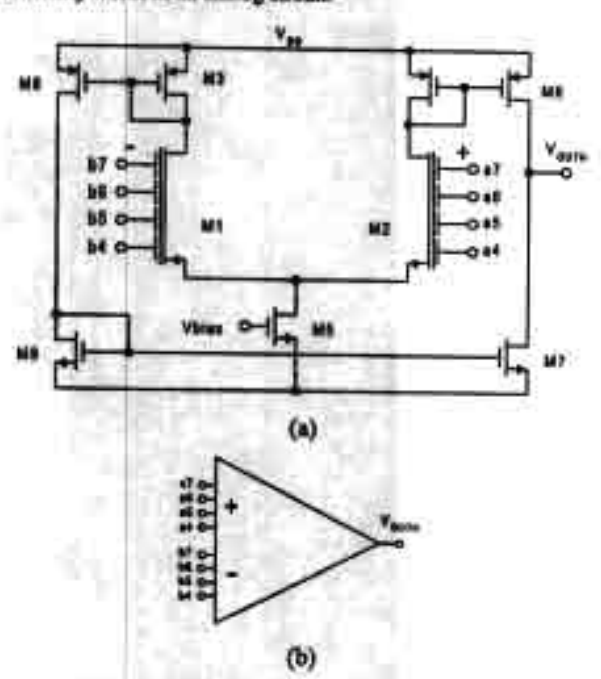


Figure 5. A Non-hysteresis 4-bit Digital Comparator

In Figure 5(a), the FGMOSs M<sub>1</sub> and M<sub>2</sub> are designed with the conventional gate areas of 12×3µm<sup>2</sup>. Let k<sub>1</sub>...,k<sub>7</sub> be the weights of the input gates denoted as a4,...,a7 and b4,...,b7 respectively, where s4 and b4 are the least significant bits of this comparator. Then the input gates have the sizes set by the binary weights as in Table 1.

Table 1. Design parameters of the FGMOS

1,56	34	ks	b6	1/2 1/2 86.6x21.8	
Binary weights	1/16	3/6	1/4		
Sizes(jum²)	10.8x22.8	21.6422.8	43.25/22.8		
Capacitance(fF)	159.7	319.5	638.9	1277.8	

This non-hysteresis 4-bit comparator can be symbolically represented as in Figure 5(b). The circuit delivers three levels of output signal at Voctor. The output is logic High or V<sub>64</sub> when the total weighted sum of the binary inputs at the positive terminal is higher than that of the negative terminal. The output is logic Low or GND when the total weighted sum of the binary inputs at the positive terminal is lower than that of the negative terminal. The output is V<sub>64</sub>/2 when the total weighted sums of the binary inputs of both terminals are equal. The latter function implies an ability to detect the equality of the binary inputs. The functionalities are confirmed by the simulation results in Figure 6.

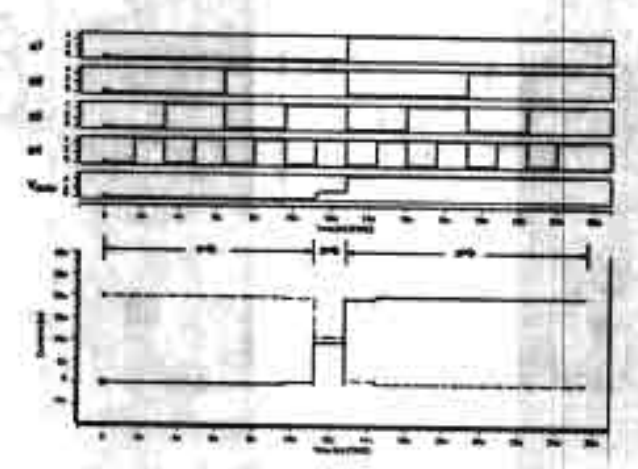


Figure 6. Results of the non-hysteresis 4-bit comparator

Figure 6 shows output signal as functions of Vourse and drain currents of the input devices where the binary a7-a4 are swept digitally and the binary b7-b4 are set to #b0111. It is seen that the output voltage is at V<sub>40</sub>/2 and the input drain currents are equal when the binary a7-a4 equals to b7-b4. This property will also be utilized further in the design of the 8-bits comparator.

The hysteresis comparator shown in Figure 7 is similar to that of Pigure 5 except that the hysteresis tuning part used in the analog comparator is employed. Because of the hysteresis operation, this circuit delivers only two levels of the output signal at high or low. As a result of the hysteresis tuning, the output signal is delivered according to the arithmetic functions of A>B or A≥B that are selected by the voltage V<sub>resc</sub>. Using the same dimensions of all MOSFETs as in Figure 5 and setting conventional gate areas of M3, M4 to 15x2.4µm², we set the input gate areas of both M3 and M4 for the input signal and for V<sub>max</sub> to 77×31µm<sup>2</sup> and 11×31µm<sup>2</sup> respectively. The simulation results are shown in Figure 8.

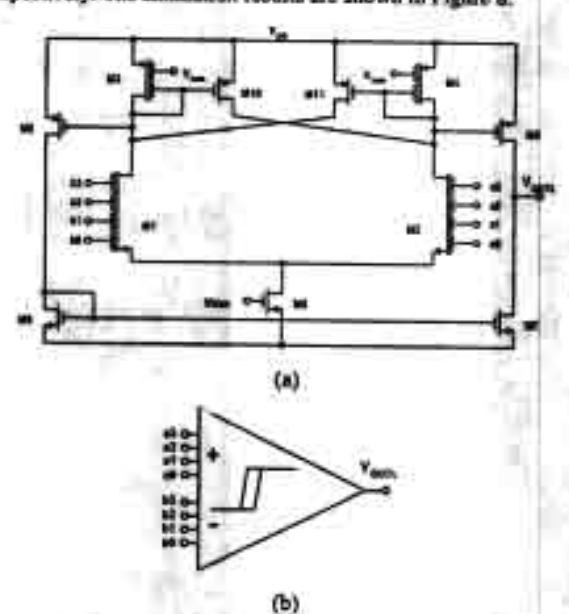


Figure 7. Hysteresis 4-bit Digital Comparator

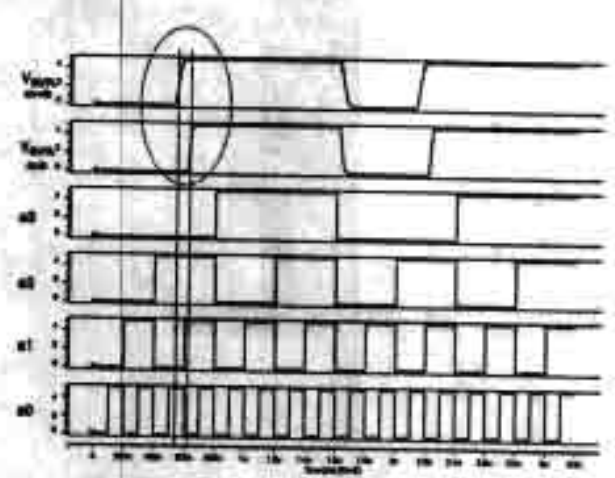


Figure 8. Simulation results of the hysteresis comparator

From Figure 8, the binary bits b3-b0 are set to #60101 while the binary bits a3-a0 are swept digitally. It is seen that if  $V_{too}$  is set to High, the output signal  $V_{OUTL}$  changes its stage when both binary sets are equal. The circuit performs the function A≥B. If V<sub>tex</sub> is set to Low, the comparator will perform the function A>B. In the next section, both hysteresis and non-hysteresis digital comparators will be combined in the design of an 8 bit digital comparator.

## 5. 8-BIT DIGITAL COMPARATOR

An 8-bit digital comparator is realized by using the two 4 bit comparators and another comparator as shown in Figure 9. The 8-bit binary inputs denoted as a7-s0 and b7-b0 can be defined as A and B respectively.

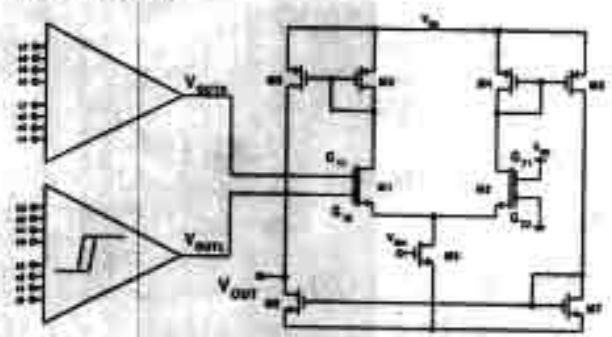


Figure 9. 8-bit digital comparator

It is seen that the 4-bit non-hysteresis comparator is used to compare the upper 4 bits where the three levels of output voltage at Vours are delivered when A>B, A<B or A=B. The 4-bit hysteresis comparator is used for the comparison of the lower 4 bits where only two levels of output voltage at Vours, are delivered. The third comparator is used as the main comparator, of which the referenced input is connected to Vot and GND. The functions of the main comparator are summarised in table 2.

Table 2. Functions of the main comparator

Upper 4 bits output	Lower 4 bits output	Output		
High / Vat	X	High/V <sub>er</sub>		
Equal / Va/2	High / V <sub>et</sub>	High / Va		
figuel / Va/2	Low/OND	Low/GND		
Low/ GND	x	Low / GND		

where X denotes don't care condition. It is seen that when the upper 4 bits of A are higher or lower than those of B, the output is High or Low immediately. If the upper 4 bits of A are equal to those of B, the output will correspond to the comparison result of the lower 4 bits of A and B. In order to have the functions correspond to Table 2, the main comparator must have the four input gates such as  $G_{11}$ ,  $G_{12}$ ,  $G_{21}$ ,  $G_{22}$  designed with proper sizes. The weights of each input are denoted as  $k_{15}$ ,  $k_{15}$ ,  $k_{21}$ ,  $k_{22}$ , correspondingly, which are considered as in table 3.

Table 3. Sizing criteria for the main comparator

log	pute	Output					
Vourse	Voun	Vour	Weight sum operations				
5V	x	5V	kH3x5+ k12x0 > k21x5+ k22x0 .:: kH > k21				
•	×	. 0	k11x0+ k12x5 < k21x5+ k22x0 k12 < k21				
2.5V	0		kf1x2.5+ kf2x0 < k21x5+ k22x0 ∴ kf1 < 2421				
2.5V	sv	5V	ki i ki 2.5+ ki 2x5 > ki i x5+ ki 2x60 .: ki i + 2-ki 2 > ki i				

where 5V and 0 stands for the logic High and Low and X denotes the don't care condition. Examining the weight sum operations, we can conclude that all weights must conform to the condition that  $k_{2l} < k_{1l} < 2k_{2l} < k_{1l} + 2k_{2l}$ . Suitable weights and sizes are summarised in Table 4.

Table 4. Design parameters of G<sub>11</sub>, G<sub>12</sub>, G<sub>21</sub>, G<sub>22</sub>

	Gii		Gu	Gu	
Binary weights	12/16	4/16	2/16	9/16	
Sines(µm²)	Sizes(jum²) 129.6x22.8		75.6x22.8	97,542.5	
Capacitanco(fF)	1916.4	638.8	1117.9	1427.3	

The functionalities can be demonstrated by the simulation results in Figure 10.

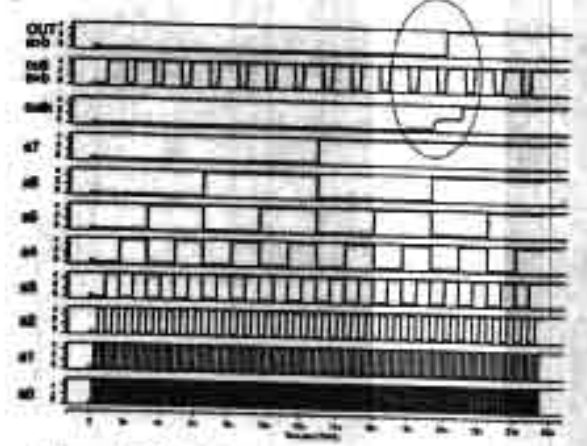


Figure 19. Simulation results of the 8-bits comparator

In Figure 10, the binary B is set to #b11000110 while the binary A is swept digitally from 0. It is seen that the Voursi of the upper comparator delivers Vou? When the upper 4-bits of the binary A equal those of B, and then the output corresponds to the Vours of the lower comparator.

## 6. CONCLUSIONS

A Hysteresis Tunable Voltage Comparator using FGMOS is proposed here. The circuit is essentially exploiting FGMOS devices in the positive feedback mode to create the hysteresis. The V<sub>Ti</sub> tuneability of the FGMOS performs the hysteresis tuning effectively. This paper also presents a design for a non-clocked 8-bit digital comparator that essentially manipulates the proposed analog voltage comparator to realize a new digital circuit in which the signal is internally processed in an analog fashion. The proposed idea can be implemented on any standard double-poly CMOS and be useful in mixed signal and computational applications. All the simulation results confirm the functionality. The design optimizations will be determined in future studies.

## 7. REFERENCES

- Linning Yin, S. H. K. Embahi, E. Sanchez-Sinencio, "A floating-Gate MOSFET D/A Converter", Proc. ISCAS'97, Vol. 1, pp. 409-412, 1997.
- [2] P. Hesler, B. A. Minch, and C. Diorio, "Floating-gate devices: they are not just for digital memories anymore", Proc. ISCAS' 99, Vol. 2, pp. 388-391, 1999.
- [3] T. S. Lande, H. Ranjbar, M. Iamail, Y. Berg, "An analog floating-gate memory in a standard digital technology", Proc., Fifth International Conference on Microelectronics for Neural Networks, pp. 271 -276, 1996.
- [4] K. Yang and A. G. Andreou, "Multiple input floating-gate MOS differential amplifiers and applications for analog computation", Proc. Midwest Symposium on Circuits and Systems, Vol. 2, pp. 1212-1216, 1993.
- [5] J. R. Angalo, S. C. Choi, G. G. Altamirno, "Low-Voltage Circuit Building Blocks Using Multiple-Input Floating Gate Transistors", IEEE trans. on Circuits and System, fundamental theory and applications, Vol. 42, No. 11, pp. 971-974, Nov. 1995.
- [6] Y. Berg, T. S. Lande, "Tunable current mirrors for ultra low voltage" Proc. ISCAS '99, Vol. 2, pp. 17-20, 1999.
- [7] T. Ohmi, T. Shibeta, "Intelligence implementation on silicon based on four-terminal device electronics", Proc. MIEL '95, Vol. 1, pp. 11-18, Sep. 1995.
- [8] H. R. Mehrvarz, C. Y. Kwok, "A large-input-dynamic-range multi-input floating-gate MOS four-quadrant analog multiplier", Digest of Technical Papers, ISSCC' 93, pp. 60 -61, 1995.
- [9] J.-J. Chen, S.-L. Liu, Y.-S. Hwang, "Low-voltage single power supply four-quadrant multiplier using floating-gate MOSFETs", Proc. ISCAS' 97, Vol. 1, pp. 237-240, 1997.
- [10] J. R. Angulo, G. Gonzalez-Altamirano and S.C. Choi, "Modeling multiple-input floating-gate transistors for analog signal processing", Proc. ISCAS' 97, Vol. 3, pp. 2020 -2023, 1997.
- [11] P. E. Allen, D. R. Hoberg, "CMOS Analog Circuit design", Oxford Press, NY, pp. 323-362, 1987.

[2] K. Moolpho, J. Ngarmnil, K. Nandhasri, "A low-voltage wide-swing FGMOS current amplifier", 2002 IEEE International Symposium on Circuits and Systems (ISCAS2002), Phoenix, May, 2002.

# A LOW-VOLTAGE WIDE-SWING FGMOS CURRENT AMPLIFIER

K. Moolpho, J. Ngarmnil and K. Nandhasri

Department of Electronic Engineering, Faculty of Engineering, Mahanakorn University of Technology, Bangkok 10530, Thailand Email: jitkasam@mut.ac.th

#### ABSTRACT

This paper proposes a new current amplifier circuit totally formed in the class AB structure utilizing CMOS inverters and the recently proposed additive analog inverter using floating-gate MOSFETs. Operating in a negative feedback topology, the amplifier can deal with wide signal swings up to ±200µA, with 1% of the THD and 10pF of C<sub>L</sub>. Designs and HSPICE simulation results are demonstrated on 0.5µm double poly CMOS processes with 1.5V and 1V power supplies to indicate high frequency and low power capabilities respectively.

## 1. INTRODUCTION

In the last decade, current-mode circuits [1] have drawn lots of interest due to their attractive features such as wide bandwidths, wide dynamic ranges and low voltage operations, all of which are very important for modern integrated circuits. Several elegant techniques for currentmode signal processing have been demonstrated successfully. These have mostly utilized current mirror cells, Gilbert gain cells and log-domain, square-root domain or translinear cells to perform filtering, multiplications, modulations, etc. For amplification purposes, current-mode amplifiers [2] based on a high open-loop current gain used for an accurate closed-loop configuration is also a very promising technique since use of a high gain device in a negative feedback loop allows large collection of transfer functions, performances of which are independent of the large but sensitive open-loop gain. So far, several high performance current amplifiers and opamps [3-9] have been proposed on CMOS technologies with various structures and topologies such as Differential Input Differential Output (DIDO), Differential Input Single-ended Output (DISO) or Single Input Differential Output (SIDO), etc. in general, the current opamp principle can be shown as a block diagram as in Fig.1, where the input current signal is firstly converted to a voltage quantity by the transimpedance amplifier (Rm) and then amplified again by the

transconductance amplifiers (Gm) to produce the output current and hence the open-loop current gain. There is usually at least one high impedance node in the circuit that should be connected by a compensation capacitor for stability.

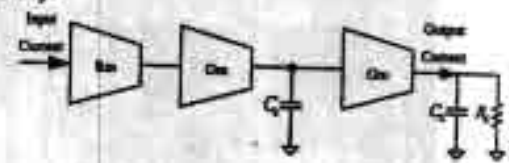
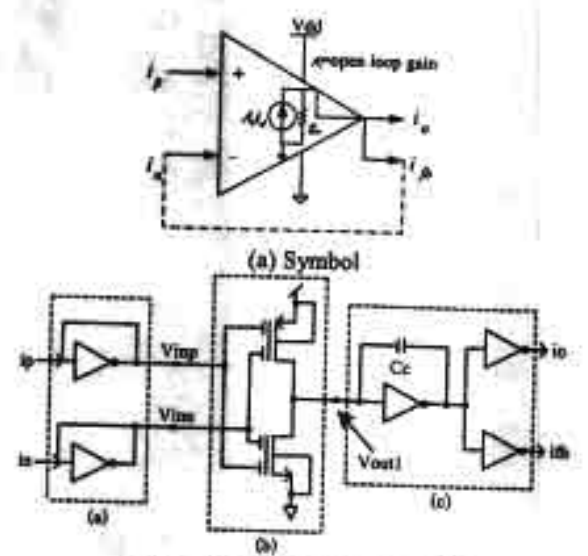


Fig.1 Current opamp principle

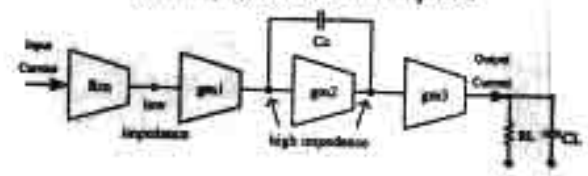
So far, most design efforts have been directed at the development of fully differential structures and enhancement of the open-loop gain and CMRR. In this work, we aim for a high signal swing by trying to avoid a class A circuit for which the limitation of current signal swing and slew rate is a result of the existing current sources, which also limit the charging current for the compensation capacitor at the high impedance node. Thus this paper proposes a new current amplifier circuit totally formed in the class AB structure utilizing CMOS inverters and the recently proposed additive analog inverter [10] using floating-gate MOSFETs. Since there is no biasing current source to limit the signal swing, our amplifier possesses a wide swing and high slew rate. The design is applied on a 0.5 µm CMOS with 1.5 Volts power supply to demonstrate high frequency operation and with 1 Volt power supply to show the feasibility of low power operations at a lower frequency range where all MOSFETs are biased in the weak inversion region.

## 2. THE PROPOSED CURRENT AMPLIFIER

The proposed current amplifier, as symbolically shown in Fig.2(a), has two identical input terminals denoted as i, and in, and two output terminals delivering the same phase of the signal denoted as i, and in, which are used as the output and the feedback post respectively. At the input terminals, it is noted that the input i, can only be symbolized as an inverting terminal when the amplifier is connected in the negative feedback configuration as shown by the dashed line. This will be discussed later in this section.



(b) The proposed current amplifier



(c) Block diagram

Fig.2 The proposed current amplifier

In Fig.2(b), the amplifier comprises three circuit blocks as shown in the dashed boxes. The transimpedance amplifier is shown in box (a) and written as

$$Rm = \frac{1}{(gm_u + gm_p)} \tag{1}$$

where gm, and gm, are respectively the transconductance of NMOS and PMOS of the inverter. The additive analog inverter in box (b) is basically a two-input CMOS inverter elegantly built from the floating-gate MOSFETs and proposed in [3]. It is employed in this circuit together with the other Rm and gm blocks to work as a differential amplifier because the polarity of in is inverse to those of incausing the voltage at node Vine to be inverse to those at node Vine. Considering only the NMOS, a large signal current equation can be written as in (2) where the coefficient of Vine is now negative.

$$I_{D} = \frac{1}{2} \mu C_{ns} \frac{W}{L} \left[ \left( k_{1} V_{inp} - k_{2} |V_{ins}| \right) - V_{5} - V_{TW} \right]^{2} (2)$$

Here k1 and k2 are the capacitive division factors [10, 11]  $C_0/C_T$  and  $C_2/C_T$ , where  $C_1$  and  $C_2$  are the effective coupling capacitances between the input gates and the floating gate and  $C_T$  is the total capacitance seen from the floating gate. All capacitances correspond directly to the sizes of the input gates and the floating gate areas obtained from the layout of the circuit. In this case, the equal input

gate areas of  $i_p$  and  $i_p$  are set and result in equal values of  $C_1$  and  $C_2$  of 50fF and k1 and k2 of 0.5. The two-inputs CMOS inverter works as if a differential amplifier for which the small signal voltage gain between the output  $V_{\rm mail}$  and the differential inputs can be derived as

$$\frac{V_{\text{med}}}{\left(V_{\text{law}} - V_{\text{law}}\right)} = -\left(gm_{\text{la}} + gm_{\text{lp}}\right)\left(r_{\text{els}} // r_{\text{elp}}\right)$$
(3)

Here r<sub>ein</sub> and r<sub>oip</sub> are the respective output resistances to the floating-gate NMOS and PMOS in the dashed box (b). With further analysis using the diagram in Fig.2(c), the open-loop current gain of the whole circuit can be derived as

$$A_i = Rm \cdot gm_1 r_{a1} gm_2 r_{a2} gm_3 \qquad (4)$$

and the dominant pole frequency(o<sub>k</sub>) is

$$\omega_d = \frac{1}{r_{cl}gm_2r_{cs}C_0}$$
(5)

while the GBW is

$$GBW = \frac{Rm \cdot gm_1 gm_3}{C_c}$$
 (6)

## 3. DESIGN AND SIMULATIONS

Based on the proposed concept, the design schematic can be simplified as shown in Fig.3, where it is seen that the circuit can be designed in a modular fashion where all inverters including the additive analog inverter have the same dimensions of NMOS and PMOS correspondingly. If a higher gain of the gm<sub>2</sub> and gm<sub>3</sub> blocks is required, we simply add more cells of the identical inverters in parallel. R<sub>C</sub> and C<sub>C</sub> are employed for the frequency compensation.

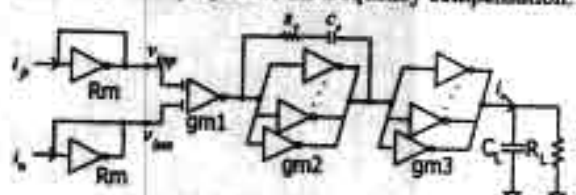
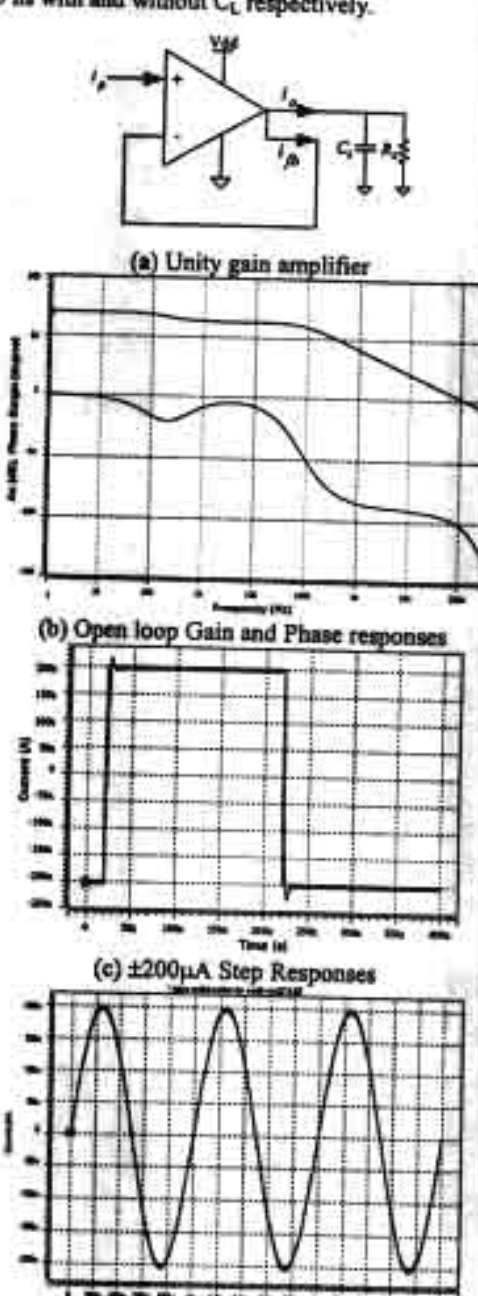


Fig.3 The design Schematic

On the Alcatel 0.5 μm CMOS process, two amplifiers have been designed for V<sub>DD</sub> of 1.5V and 1V to demonstrate high frequency operations and low power respectively. With V<sub>DD</sub> of 1.5V, all NMOS and PMOS are designed with the dimensions of 6.9/0.5 and 23.6/0.5 respectively resulting in the idle currents of 30 μA for each inverter. As seen in Fig.3, only one CMOS inverter is employed for each Rm and gm1 block but extra input gates on Poly2 are connected to the inverter of the gm1 block. Then four and three inverters connected in parallel are employed for the gm2 block and the gm3 block respectively. The amplifier is loaded with C<sub>L</sub> of 10 pF and R<sub>L</sub> of 1.69k Ω that is the same value as Rm or its input resistance. To improve the phase

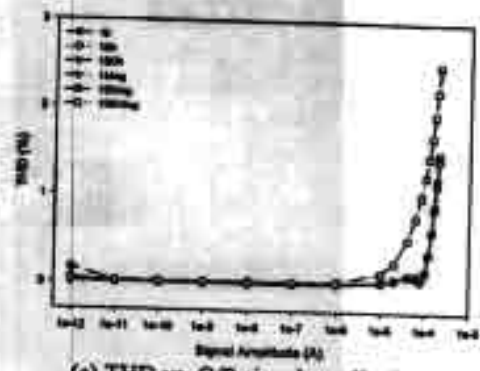
margin, R<sub>C</sub> of 1k Ohms and C<sub>C</sub> of 0.8pF are also included in the compensation scheme. The circuit was simulated on HSPICE with the performances shown in Fig.4 where 69.6dB Open-loop gain, 127MHz GBW and 74° Phase margin were achieved with a supply voltage of 1.5Volts and 635μW of power consumption. As a unity gain buffer, step response and linearity were measured at the maximum signal amplitude of ±200μA and are shown in Fig.4(d) and (e) where the 1% settling times are measured as 9.4 and 34.5 ns with and without C<sub>L</sub> respectively.



(d) ±200µA Signal Swings of O/P vs. I/P

33.1

IV - 661



(e) THD vs. O/P signal amplitude

Fig.4 Simulation results

Another amplifier with a 1V power supply was designed including all NMOS and PMOS with the dimensions of 8/0.5 and 19.9/0.5 respectively operated in the weak inversion region. As in Fig.3, only one CMOS inverter is employed for each Rm and gml block. Then five and two inverters connected in parallel are employed for the gm<sub>2</sub> block and the gm, block respectively. The amplifier is loaded with Ct of 10pF and Rt of 47.86kQ. From simulations, an open-loop gain of 68.3dB, with 2.68MHz GBW and 68° phase margin is achieved with 6µW power consumption. Due to space restrictions, not all performance graphs could be included here. However, in Table 1 all performances are compared with those of some earlier designs. The 1.5V Vop version amplifier is also tested in negative feedback structure with passive networks to set the closed loop gains higher than I as shown in Fig.5.

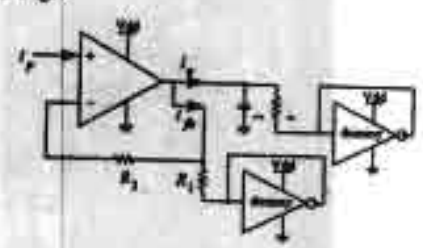


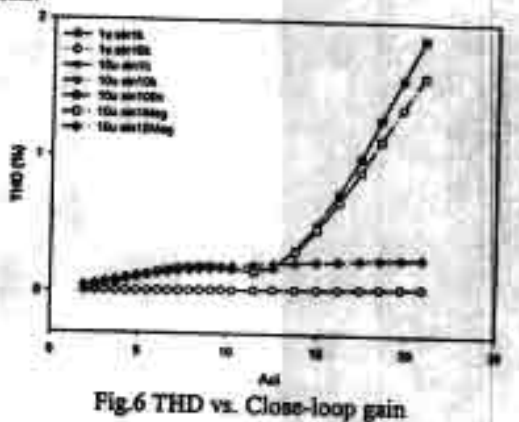
Fig.5 The amplifier in negative feedback

Fig.5 displays a non-inverting amplifier with a resistive negative feedback network. We arbitrarily put the dummy shorted input-output inverters to work as resistive loads and also to set the DC offset voltage to half of the Von which is the same DC voltage at all input and output nodes. Then the closed loop gain can be derived as

$$A_{cs} = 1 + \frac{R_2 + Rm}{R_1 + Rm} \tag{7}$$

where  $R_1$  and  $R_2$  are the resistances in the range of 0- $10k\Omega$  which are integrable value on a chip. The dummy inverter load is used to settle a proper do level in order to avoid DC offset of the feedback current. From (7), Rm

with R<sub>i</sub> is the transimpedance of the dummy inverter while Rm with R2 is the input resistance of the i, terminal. Hence all Rms are the same value. With Vpp of 1.5V, by setting  $R_1$  at  $10\Omega$  and adjusting  $R_2$  for various close-loop gains, the THD of the O/P signal were measured and shown in Fig.6 where the labels in the plot show details of the input signals.



## 4. CONCLUSION

This paper has proposed a new low voltage wide swing current amplifier that can receive a signal swing as large as ±200µA amplitude while a THD of about 1% is still maintained. The circuits can totally be realized in the class AB thanks to the use of CMOS inverters and the available additive unalog inverter cells using floating-gate MOSFETs. An effect of complex poles and zeros around the 100Hz of the open loop gain in Fig.4 (a) can be noticed as a result from the coupling capacitors of the FGMOS devices. A deep analysis will be placed as future works. In this paper, the circuit is called a current

amplifier instead of opamp due to the lack of CMRR capability, which will be part of our future works.

## 5. REFERENCES

[1] C. Toumazou, F.J. Lidgey, D. Haigh, "Analogue IC Design:

The current-mode Approach", Peregrinus, UK, 1990.
[2] G. Palmisano, G. Palambo, S. Pennisi, "CMOS Current Amplifiers", Kluwer Academic Publishers, 1999.

[3] E. Aben-Allam, E.I. El-Marry, "A 200 MHz Steered current operational amplifier in 1.2-um CMOS Technology", IEEE J. Solid-State Circuits, vol. 32, 1997, pp. 245-249

[4] S. Jan, D.M. Kim, "Fully differential current operational amplifier", Elec. Lett., vol. 34, 1998, pp. 62-63.

[5] G. Palmirano, S. Pennisi, "Low-Voltage continuous-time CMOS current amplifier with dynamic bissing", Proc. ISCAS2001, pp. I-312-I-315.

[6] R.H. Zele, S. Lee, D.J. Allstot, "A high gain current-mode operational amplifier", Proc. ISCAS92, pp. 2852-2855.

[7] T. Kaufberg, "A CMOS current-mode operational amplifier", IEEE J. Solid-State Circuits, vol. 28, 1993, pp. 849-852.

[8] E. Brunn, "A high-speed CMOS current-mode op-amp for very low supply voltage operation", Proc. ISCAS94, pp.509. 512.

[9] E. Abou-Allam, E.I. El-Masry, "High CMRR CMOS current rational amplifier", Elec. Lett., vol. 30, 1994, pp. 1042-1043. [10] Y. Berg, O. Naese, M. Hovin, "Ultra low voltage floatinggate transcenductance amplifier with tunable gain and linearity", Proc. ISCAS2000, pp. III-343-346.

[11] T. Shibata, T. Ohmi, "A Functional MOS Transistor Featuring Gute-Level Weighted Sum and Threshold Operations", IEEE Trans. Elec. Devices, vol. 39, 1992, pp. 1444-1455.

Acknowledgement: This work has been supported by a grant from the Thailand Research Fund (TRF). Authors would like to thank the TRF for their precious support.

TABLE 1 PERFORMANCE COMPARISONS

			25.3		Chico Gora	79 Charles (Date)		<b>WATER</b>	140			
COA	[3]±	[3]@	[4]±	[5]±	[6]±	[6]@	1716	[81±	(91±	Dec	posed	***
Years	1997	1997	1998	2001	1992	1992	1993	1994				Unit
DC Gain	65	70	53	80	65	54			1994		001	
UGBW	200	210	300	16	9	90	72	94.2	67	69.6	68.3	dB
PM	60	>45	50	68	60	60	3	65	100	127	2.58	MH
Input Resistance	0.147	2	21	-	_	00	60	-40	61	74	60	
Output Resistance		-	-	NA.	3.65	5	NA	5.8	316	1.68	47.86	ΚΩ
	2.8	-	0.597	NA	0.899	0.186	NA	7.6	0.3	0.09	0.847	MO
Settling Time (1%)	5.1	NA	7.1	100	150	15	NA	NA.	NA	34.5*	240*2	-
Slow rate +/-	NA	NA	NA	+0.4	NA	NA	NA	NA	NA	+145/	+0.078/	Πε μΑ/n
Re	NA:	NA	NA.	NA	NA	NA	NA	NA	NA	-170	-0.1	
Ce	NA	NA	NA	1.5	10	1.25	100	-			0.9	KΩ
RL	NA	NA	NA	1	NA	-	111	NA	NA	0.8	1	pF
CL	NA.	NA	NA	-57.5	100	NA	NA	NA	NA	1	2.5	ΚΩ
Power Dissipation	NA	-	-	NA	NA	NA	NA	NA	NA	16	10	pF
	-	4.5	<0.86	NA	3.1	4.6	NA	0.03	4.5	0.635	0.006	mW
Technology(CMOS)	1.2	1.2	0.6	0.8	2	2	2.4	2	1.2	0.5	0.5	_
Supply	+3	±3	3	1.2	NA	NA	NA	NA I	1	15	1.0	μm V

± = Simulation results, ⊗ = Measured results, NA = not available, \* = at ±200µA step i/p, \* = at 4µA step i/p

[3] K. Nandhasri, J. Ngarmnil, K. Moolpho, "A 2.8V RWDM BTL Class-D Amplifier using an FGMOS Comparator", 2002 IEEE International Symposium on Circuits and Systems (ISCAS2002), Phoenix, May. 2002.

# A 2.8V RWDM BTL CLASS-D POWER AMPLIFIER USING AN FGMOS COMPARATOR

K. Nandhasri, J. Ngarmnil and K. Moolpho

Department of Electronic Engineering, Faculty of Engineering,
Mahanakorn University of Technology, Bangkok 10530, Thailand
Phone & Fax (662) 9883655 Ext.239, Email: kristana@mut.ac.th, jitkasam@mut.ac.th

#### ABSTRACT

This paper presents a design of an output stage based on Class-D amplifier techniques using Rectangular Wave Delta Modulation (RWDM) topology. This amplifier has a simple structure comprised only of a hysteresis comparator and output drivers. Thanks to the use of a multiple inputs hysteresis comparator using floating-gate MOSFETs, the amplifier is capable of low voltage operations. On Alcatel 0.5µm double poly CMOS process, this amplifier demonstrated to deliver up to 0.88Watts with 95% efficiency with a 2.8 Volts power supply. This means implementation as a monolithic chip is possible, making this amplifier suitable for portable applications such as speaker driving circuits in mobile phones, hearing aids and other implantable medical devices.

## 1. INTRODUCTION

Many audio power amplifiers are designed in class-A or class-AB, and so they normally deliver a limited efficiency because their power transistors operate in the linear area where a huge biasing or idle current is normally consumed in order to be able to deliver enough power to the loads. This then results in excessive power dissipation or heat. In order to improve the efficiency, switching converter techniques such as Pulse Width Modulation (PWM) can be applied to the development of audio amplifiers, referred to as switching amplifiers or class-D type [1,2]. This type of amplifier presents several advantages over conventional class-A or AB amplifiers in their high efficiency and low internal power dissipation. In this work we present the development of a class-D amplifier based on the RWDM technique [3] utilizing a multiple input hysteresis voltage comparator using floating-gate MOSFETs to allow low voltage operation for the amplifier. The circuit is then suitable for production as a monolishic chip for battery-operate applications such as speaker driving circuits in mobile phones, hearing aids and other implantable medical devices. Designs and simulation results will be discussed in detail below,

## 2. CLASS-D AMPLIFIER

Conventionally, most class-D amplifiers are based on the Pulse Width Modulation (PWM) technique where the pulse width of the output PWM signal produced is proportional to the amplitude of the modulating signals between the audio input signal and the triangular signal. The signal at the output is recovered from the PWM signal by a low pass filter, which could be formed by a loaded resistor and an inductor inherently obtained from carphones or speakers. Fig.1 shows the basic building blocks of a conventional class D amplifier comprising triangular waveform generator, comparator and output driving stage.

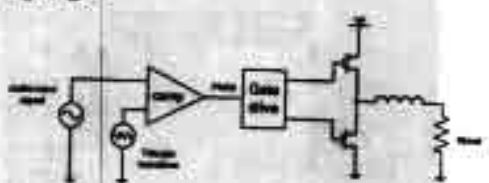


Fig. 1 Conventional PWM class-D amplifier

From Fig.1, the comparator compares the audio signal input with the triangular waveform from the waveform generator to produce a PWM signal, which is then used to control the switching timing of the output stage transistors to drive a low impedance load. The output power delivered to the load is proportional to the average output current controlled by the duty cycle of the PWM signal. The duty cycle is 50% when there is no signal at the input, thus the average output voltage is zero. PWM class-D amplifiers can dissipate less power by properly arranging the switching timing of the output power MOSFETs between the two lowest-dissipation modes such as fully on and fully off.

Another promising technique used in class-D amplifiers is the RWDM principle shown in Fig.2. In concept RWDM is similar to PWM except that the input signal denoted as  $V_n(t)$  is compared with the feedback signal  $V_n(t)$  which is essentially the integrated signal of RWDM by a low-pass filter. Hence loading conditions from the loads are taken into account to control the RWDM signal and then to control the output power. Since there is a hystoresis in the

comparator,  $V_a(t)$  can track the amplitude of  $V_a(t)$  within the  $\pm \Delta V$  boundary as shown in Fig.2.

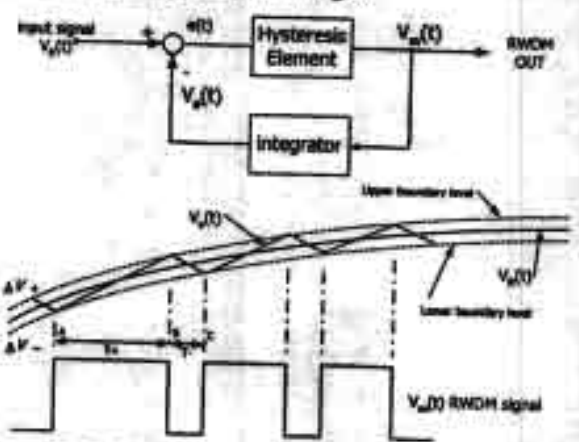


Fig. 2 Block diagram of the RWDM technique

Based on the RWDM mechanism in Fig.2, the switching frequency of the RWDM output signal can be calculated as in (1)

$$f = \frac{1}{T} = \frac{S_c}{4\Delta V} \left[ 1 - \left( \frac{S_s(t)}{S_c} \right)^2 \right]$$
 (1)

where  $S_R$  and  $S_C$  denote the slopes of the input signal  $V_R(t)$  and the feedback signal  $V_r(t)$  respectively and  $\Delta V$  is the tracking boundary corresponding to the magnitude of the hysteresis loop which is controlled directly by the trip voltage of the hysteresis comparator.  $S_C$  is also controlled by the time constant of the integrator in the feedback path.

## 3. THE PROPOSED RWDM CLASS-D AMPLIFIER

A new proposed class-D amplifier based on the RWDM technique is presented as a block diagram in Fig.3, where it is seen that the amplifier comprises only a hysteresis comparator, driving circuits and an integrator formed by the resistor inductor low-pass network. The circuit can be integrated onto a monolithic chip except for the inductor and the load resistor.

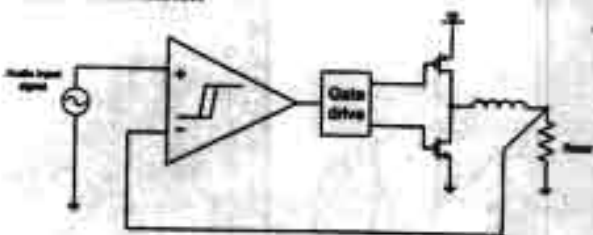


Fig.3 The Proposed Concept

From Fig.3 the audio input signal is directly connected to the input of the comparator, which is basically a high impedance node since it is the input gate of a MOSFET. Hence no loading of the signal source occurs. The comparator then compares the input signal with the feedback signal from the output. With the built-in hysteresis loop, the comparator can produce the output RWDM signal comprising only logic low or high that is then integrated by the inductor resistor network. The feedback signal as a saw-tooth-like signal is then used to compare with the input signal in the next cycle.

## 3.1 The Hysteresis Comparator

The hysteresis can be shown as the range between V<sub>TRP</sub>, and V<sub>TRP</sub>, as in Fig.4. In this paper, we expand the switching range of a hysteresis comparator to control the amount of output ripple and switching frequency of the Class-D amplifier.

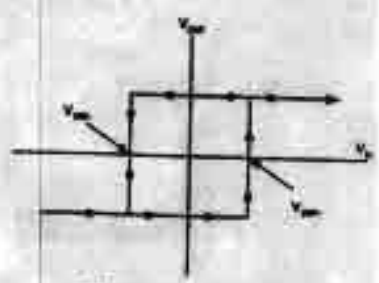


Fig.4 Hysteresis loop

An example of the hysteresis comparator [4, 5] is shown in Fig.5, where it is seen that the hysteresis is generated from a positive feedback produced by M10 and M11. The positive feedback occurs only when the current ratio of Ippo/Ipp or Ippi/Ipp is greater than one.

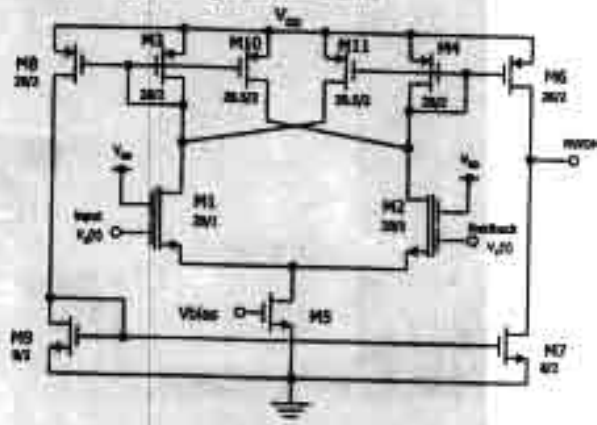


Fig. 5 Rail to rail input hysteresis comparator

The hysteresis comparator abown in Fig.5 is able to receive a wide-range input signal. This particular ability is

achieved by the employment of the two-inputs floatinggate MOSFETs (FGMOS) [5, 6] as the input transistors M1 and M2 of the differential amplifier. This characteristic allows the feedback signal at the gate of M2 to track the amplitude of the input signal at the gate of M1 effectively between the supply voltage and ground. Hence low voltage operation is possible. This is results because one of the input gates of both M1 and M2 are connected to Vdd, so both FGMOSs M1 and M2 are ensured to be be turned on at all levels of the input signal. In other words, the comparator basically possesses the rail-to-rail characteristic.

## 3.2 FGMOS Basic Principles

FGMOS is an ordinary MOSFET except that the gate, which is built on the conventional polyl, is floating and then called 'Floating-Gate'. The structure of FGMOS is shown in Fig.6.

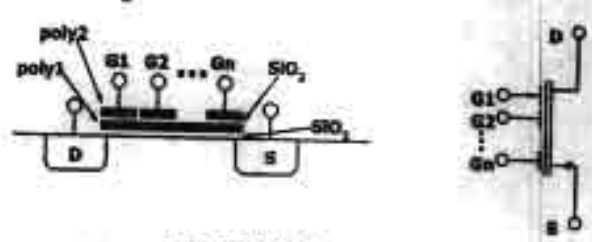


Fig.6 FGMOS structure

A multiple input MOSFET based on the FGMOS structure [6,7] is shown in Fig.6. It comprises the floating gate, and input gates (G1, G2) built on Poly2, which are coupled to the Poly1 gate by the capacitors between Poly1 and Poly2 denoted as  $C_1$  and  $C_2$ . Assuming zero initial charge on the floating-gate, the drain current can be written as

$$I_0 = \frac{1}{2} \mu C_{oc} \frac{W}{L} [(k_1 V_{o1} - V_z) - (V_{fN} - k_1 V_{o2})]^2$$
 (2)

$$I_{b} = \frac{1}{2} \mu C_{so} \frac{W}{L} \left[ \left( k_{i} V_{ci} + k_{2} V_{ci} \right) - V_{i} - V_{iv} \right]^{2}$$
 (3)

where  $k_1$  and  $k_2$  are  $C_1/C_7$  and  $C_2/C_7$  respectively and  $C_7$  is the total capacitance of the floating gate. The drain current is essentially a linear sum of all inputs weighted by the capacitive coupling ratios. Equation (2) is arranged to show the threshold operation with only two input gates assumed. It is seen that  $V_{CI}$  can be utilized as a signal port while  $V_{CI}$  is used to tune the effective threshold voltage. Equation (3) is written to show a linear sum of the weighted multiple-input voltages. This operation ensures the comparator has the capability to handle large input signal swings while it still operates in the saturation region as mention before,

## 4. THE PROPOSED RWDM BTL CLASS-D

A Bridge Tied Load (BTL) class-D amplifier based on the RWDM technique is presented in Fig.7. It is basically a fully differential version of the proposed RWDM concept shown in Fig.3. With the BTL configuration the output voltage swing can be double those of the half-bridge configuration in Fig.3. The audio input signal is directly connected to the input of the comparator, which is normally in the range of 0-V<sub>DO</sub> so we use 3-inputs floating-gate MOSFETs as the input differential pairs of the hysteresis comparator.

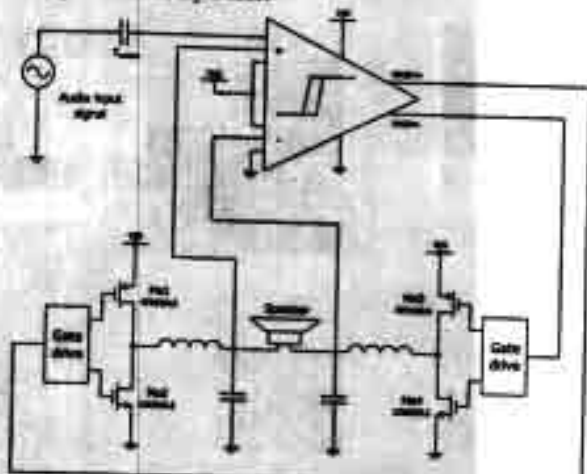


Fig.7 The proposed RWDM BTL class-D amplifier

In Fig.8, the 3-inputs fully differential hysteresis comparator comprises three-input gates FGMOS devices as the differential pairs of which the coupling capacitors are designed as C,-200fF, C,=128fF and C,-64fF which correspond to the capacitive coupling ratios of k1, k2 and k3 to 0.5, 0.32 and 0.16 respectively. The first inputs of both plus and minus terminals having the weight factor of 0.5 are connected to V<sub>DD</sub> to bias the differential pairs. This results in a DC potential of 0.5Vpp at the floating-gate on Polyl of the differential pairs. The 2rd input gates having weight of 0.32 are used as the inputs of the comparator while the 2<sup>nd</sup> gate of M1 is connected to the AC-coupled audio input signal and the 2<sup>nd</sup> gate of M2 is connected to Gnd. The weights of the 2<sup>nd</sup> inputs allow a wide input swing for the comparator. The 3rd input gates with the weight of 0.16 are connected to output nodes of the amplifier respectively. They are designed with half of the weight factor of the 2" gates in order to make the close loop gain of the amplifier equal to 2, which is the requirement to have an output signal swing of +/- 2.8V while the input signal swing is only in the range 0-2.8V. The other advantage of this fully differential comparator is that the RWDM output signals from the comparator are exactly out of phase without any delay. The control of the

power MOSFETs of both sides of the loads will be very precise. Dimensions of all MOSFETs are also shown in the figure.

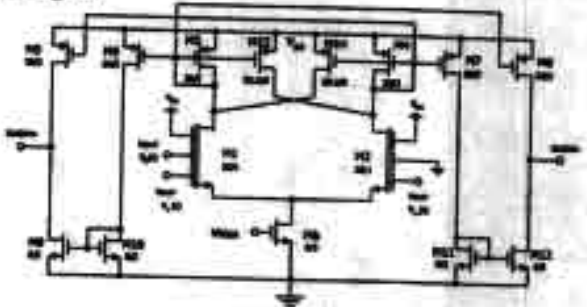


Fig.8 Fully differential comparator

## 5. SIMULATION RESULTS

Based on the proposed circuit in Fig.7, the amplifier has been designed on Alcatel 0.5µm CMOS process with 2.8 Volts power supply. The amplifier can deliver current to the  $8\Omega$  resistive loads and correspond to the output signal of 5.2V<sub>pp</sub>. Other performances based on simulation results on HSPICE are summarized in Table 1.

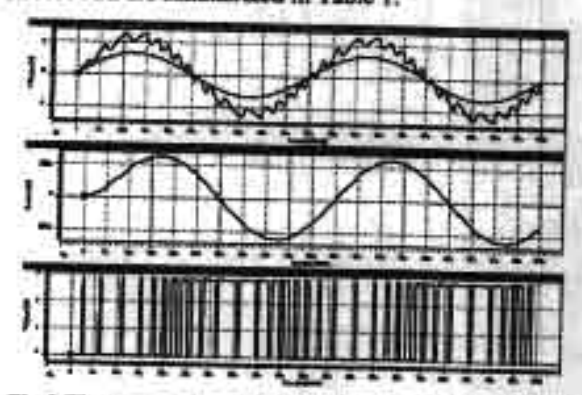


Fig.9 The voltage output signal, the current output signal and the RWDM output signal at input 1.3V, 20kHz

Table 1 Summary of the proposed amplifier

Process technology	Alcatel 0.5µm CMOS
Supply voltage	2.8V
Static Power dissipation	79.51µW
Maximum output swing	5.2V.
Output load	8Ω
Maximum power	0.88W
Efficiency	95%

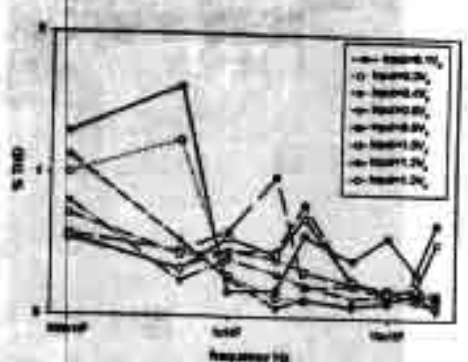


Fig. 10 THD vs. Signal frequency and input amplitude

## 6. CONCLUSIONS

A single-chip low-voltage high-efficiency Class-D Power Amplifier for portable devices has been proposed The amplifier has a very simple architecture that makes it essier for it to be integrated with other circuit blocks on a system level. By virtue of the high efficiency of Class-D architecture coupled with the low voltage operation provided by the use of floating-gate MOSPET hysteresis comparator, this amplifier is suitable for portable devices with battery operations. It exhibits high distortion at low input signal due to the small changing of the input signal compared to the ripple at the output. The efficiency of this circuit is 95% at 0.88Wart with a 2.8V power supply.

#### 7. REFERENCES

[1] D. L. Schilling, C. Belove, "Electronic Circuits Discrete And Integrated", 3rd edition, McGraw-Hill, 1989.

[2] B. Duncan, "High Performance Audio Amplifiers", Newnes,

[3] L. Kirjalek, P. Pawawongsak, "DSP Application for RWDM Inverters", The 22" Electrical Engineering Conference, Bangkok, 1999, pp. 541-544.

[4] P.E. Allen, D.R. Hoberg, "CMOS Analog Circuit design", Conference, Bangkok, 1999, pp. 541-544.

Oxford Press, NY, 1987, pp.323-362.

[5] K. Nandhaeri, J. Ngarmuil, "Designs of Analog and digital Comparators with FGMOS", Proc.ISCAS2001, Vol.1, pp. 25-28. [6] K. Yang and A. G. Andreou, "Multiple input floating-gate MOS differential amplifiers and applications for analog computational", Proc. MWSCA5, Vol.2, 1993, pp. 1212-1216.

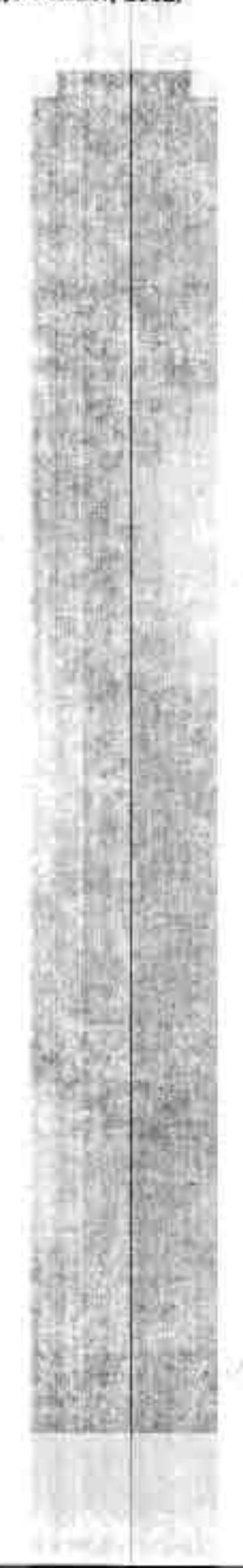
J. R. Angulo, G. Gonzalez-Altamirano and S.C. Choi,
 "Modeling multiple-input floating-gate transistors for analog signal processing", Proc. ISCAS97, Vol. 3, pp. 2020 -2023.
 Sung-Mo Kang, Yusef Leblebici, "CMOS digital integrated

circuits analysis and design", McGraw-Hill, 1996.

[9] Choi et al, "A design of a 10-W single-chip class D Audio amplifier with very high efficiency using CMOS technology". IEEE Trans. Consumer Electronics, Vol. 45, No.3, Aug 1999.

Acknowledgement: This work has been supported by a grant from the Thailand Research Fund (TRF). The authors would like to thank the TRF for their precious support.

[4] J. Ngarmnil, K. Nandhasri, K. Moolpho, "Floating-gate MOSFETs Analog Circuit Building Blocks: Design perspective", 2002 IEEE International Symposium on Communication and Information Technology, October, 2002.



## FLOATING-GATE MOSFETS ANALOG CIRCUIT BUILDING BLOCKS: DESIGN PERSPECTIVE

J. Ngarmuil, K. Nandhasri and K. Moalpho

Department of Electronic Engineering, Faculty of Engineering, Mahanakom University of Technology, Bangkok, 10530, Thailand Email: jitkasam@mut.ac.th

### ABSTRACT

Floating-gate MOSFET on a standard double-poly CMOS offers various new useful functions which can be used to create many novel circuits in both analog and digital circuits. This paper reviews some recently proposed FGMOS circuits, such as a hysteresis tunable voltage comparator, analog-based digital comparators, a low-voltage class AB current-mode amplifier circuit and its filtering application. Designs and HSPICE simulation results are demonstrated on standard double poly CMOS processes.

#### 1. INTRODUCTION

Recently, many applications of Floating gate MOSFET or FGMOS devices in analog circuits have been reported [1-6]. Normally playing a key role in modern integrated memories such as EEPROM and Flash, FGMOS has some unique characteristics which could be applied to design many new circuits or to enhance existing analog circuits for having extra special features such as very low voltage, low power and high complexity functions. This paper reviews the recently proposed analog and digital comparators based on an exploitation of the FGMOS. First, a hysteresis tunable analog comparator is constructed with an electronically tunable positive feedback factor obtained by threshold voltage tuning of the embedded FGMOS devices. Then, digital comparators are developed by essentially modifying the proposed analog voltage comparator to be a new digital circuits in which signal are internally processed with analog mechanism. Moreover, a high open-loop gain current amplifier circuit totally formed in the class AB structure utilizing CMOS inverters and floating-gate MOSFETs is also reviewed with its attractive features such as wide bandwidths, wide dynamic ranges and low voltage operations. Based on the high open loop gain amplifier, a single amplifier biquad is designed and demonstrated as an application of the proposed current amplifier.

### 2. FGMOS BASIC PRINCIPLE

FGMOS is an ordinary MOSFET except that the gate, which is built on the conventional polyl, is floating and then called 'Floating-Gate'. The structure of FGMOS is shown in Fig. 1.

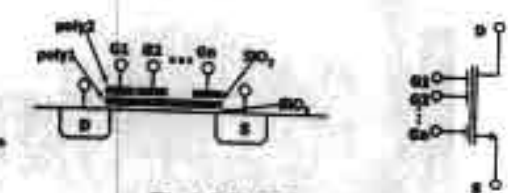


Fig.1 FGMOS structure

A multiple input MOSPET based on the FGMOS structure [2-3] is shown in Fig.1, which is seen that it comprises the floating gate, and input gates  $(G_1,...,G_n)$  built on Poly2, which are coupled to the Poly1 gate by the capacitors between Poly1 and Poly2 denoted as  $C_1,...,C_n$ . Assumed with the zero initial charge on the floating-gase and only two input gates, the drain current can be written as

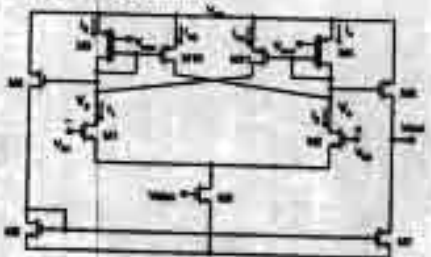
$$\hat{I}_{b} = \frac{1}{2} \mu C_{ac} \frac{W}{L} \left[ \left( k_{i} V_{a1} - V_{a} \right) - \left( V_{rac} - k_{a} V_{a3} \right) \right]^{2}$$
 (1)

$$I_{p} = \frac{1}{2} \mu C_{m} \frac{W}{L} \left[ \left( k_{1} V_{G1} + k_{2} V_{G2} \right) - V_{g} - V_{D1} \right]^{g}$$
 (2)

where  $k_1$  and  $k_2$  are capacitive coupling ratios  $C_0/C_T$  and  $C_2/C_T$  respectively and  $C_T$  is the total capacitance of the floating gate. The drain current is essentially a linear sum of all inputs weighted by the ratios. Equation (1) is arranged to show the threshold voltage tuning. It is seen that  $V_{01}$  can be utilized as a signal port while  $V_{02}$  is used to tune the effective threshold voltage. Equation (2) is written to show a linear sum of the weighted multiple-input voltages.

### 1. HYSTERESIS TUNABLE COMPARATOR

A hysteresis tunable comparator was proposed in [7], based on an electronically tunable positive feedback factor produced by threshold voltage tuning of the embedded FGMOS devices.



Flg.2 Hysteresis Analog Comparator

power MOSFETs of both sides of the loads will be very precise. Dimensions of all MOSFETs are also shown in the figure.

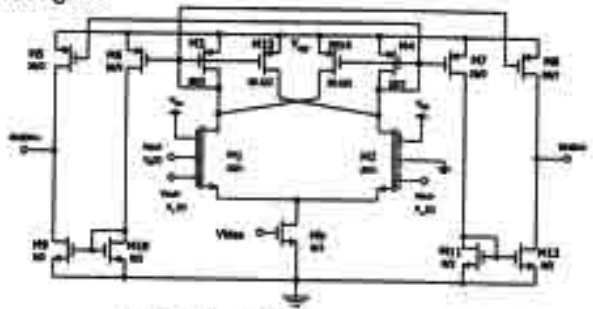


Fig.8 Fully differential comparator

### 5. SIMULATION RESULTS

Based on the proposed circuit in Fig.7, the amplifier has been designed on Alcatel 0.5μm CMOS process with 2.8 Volts power supply. The amplifier can deliver current to the 8Ω resistive loads and correspond to the output signal of 5.2V<sub>pp</sub>. Other performances based on simulation results on HSPICE are summarized in Table 1.

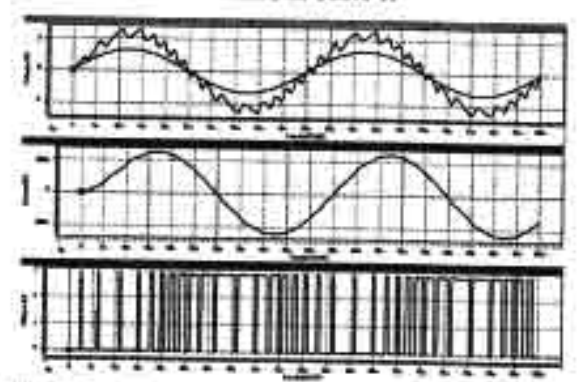


Fig.9 The voltage output signal, the current output signal and the RWDM output signal at input 1.3V<sub>2</sub>, 20kHz

Table 1 Summary of the proposed amplifier

Process technology	Alcatel 0.5µm CMOS				
Supply voltage	2.8V				
Static Power dissipation	79.51µW				
Maximum output swing	5.2V <sub>p-0</sub>				
Output load	8Ω				
Maximum power	0.88W				
Efficiency	95%				

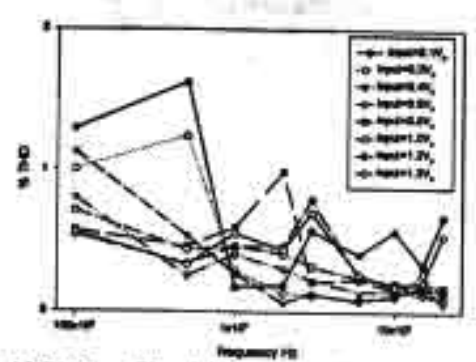


Fig.10 THD vs. Signal frequency and input amplitude

### 6. CONCLUSIONS

A single-chip low-voltage high-efficiency Class-D Power Amplifier for portable devices has been proposed The amplifier has a very simple architecture that makes it easier for it to be integrated with other circuit blocks on a system level. By virtue of the high efficiency of Class-D architecture coupled with the low voltage operation provided by the use of floating-gate MOSPET hysteresis comparator, this amplifier is suitable for portable devices with battery operations. It exhibits high distortion at low input signal due to the small changing of the input signal compared to the ripple at the output. The efficiency of this circuit is 95% at 0.88Watt with a 2.8V power supply.

### 7. REFERENCES

 D. L. Schilling, C. Belove, "Electronic Circuits Discrete And Integrated", 3rd edition, McGraw-Hill, 1989.

[2] B. Duncan, "High Performance Audio Amplifiers", Newnes, 1996.

[3] L. Kitjalak, P. Pawawongsak, "DSP Application for RWDM Inverters", The 22<sup>nd</sup> Electrical Engineering Conference, Bangkok, 1999, pp. 541-544.

[4] P.E. Allen, D.R. Hoberg, "CMOS Analog Circuit design", Oxford Press, NY, 1987, pp.323-362.

[5] K. Nandhasri, J. Ngarumil, "Designs of Analog and digital Comparators with FGMOS", Proc.ISCAS2001, Vol.1, pp. 25-28, [6] K. Yang and A. G. Andreou, "Multiple input floating-gate MOS differential amplifiers and applications for analog computational", Proc. MWSCAS, Vol.2, 1993, pp.1212-1216.

[7] J. R. Angulo, G. Genzalez-Altamirano and S.C. Choi, "Modeling multiple-input floating-gate transistors for analog signal processing", Proc. ISCAS97, Vol. 3, pp. 2020 -2023.

[8] Sung-Mo Kang, Yusef Leblebici, "CMOS digital integrated circuits analysis and design", McGraw-Hill, 1996.

[9] Choi et al, "A design of a 10-W single-chip class D Audio amplifier with very high efficiency using CMOS technology", IEEE Trans. Consumer Electronics, Vol. 45, No.3, Aug 1999.

Acknowledgement: This work has been supported by a grant from the Thailand Research Fund (TRF). The authors would like to thank the TRF for their precious support.

[4] J. Ngarmnil, K. Nandhasri, K. Moolpho, "Floating-gate MOSFETs Analog Circuit Building Blocks: Design perspective", 2002 IEEE International Symposium on Communication and Information Technology, October, 2002.

# FLOATING-GATE MOSFETS ANALOG CIRCUIT BUILDING BLOCKS: DESIGN PERSPECTIVE

J. Ngarmnil, K. Nandhasri and K. Moolpho

Department of Electronic Engineering, Faculty of Engineering, Mahanakom University of Technology, Bangkok, 10530, Thailand Email: jitkasam@mat.ac.th

### ABSTRACT

Floating-gate MOSFET on a standard double-poly CMOS offers various new useful functions which can be used to create many novel circuits in both analog and digital circuits. This paper reviews some recently proposed FGMOS circuits, such as a hysteresis tumble voltage comparator, analog-based digital comparators, a low-voltage class AB current-mode amplifier circuit and its filtering application. Designs and HSPICE simulation results are demonstrated on standard double poly CMOS processes.

### 1. INTRODUCTION

Recently, many applications of Floating-gan MOSFET or FGMOS devices in analog circuits have been reported [1-6]. Normally playing a key role in modern integrated memories such as EEPROM and Flash, FGMOS has some unique characteristics which could be applied to design many new circuits or to enhance existing analog circuits for having extra special features such as very low voltage, low power and high complexity functions. This paper reviews the recently proposed analog and digital comparators based on an exploitation of the FGMOS. First, a hysteresis tunable analog comparator is constructed with an electronically tunable positive feedback factor obtained by threshold voltage tuning of the embedded FGMOS devices. Then, digital comparators are developed by essentially modifying the proposed analog voltage comparator to be a new digital circuits in which signal are internally processed with analog mechanism. Moreover, a high open-loop gain current amplifier circuit totally formed in the class AB structure utilizing CMOS inverters and floating-gate MOSFETs is also reviewed with its attractive features such as wide bandwidths, wide dynamic ranges and low voltage operations. Based on the high open loop gain amplifier, a single amplifier biquad is designed and demonstrated as an application of the proposed current amplifier.

### 2. FGMOS BASIC PRINCIPLE

FGMOS is an ordinary MOSFET except that the gate, which is built on the conventional polyl, in floating and then called 'Floating-Gate'. The structure of FGMOS is shown in Fig. 1.

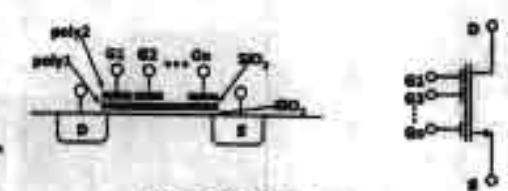


Fig.1 FGMOS structure

A multiple input MOSPET based on the FGMOS structure [2-3] is shown in Fig.1, which is seen that is comprises the floating gate, and input gates (G<sub>1-1</sub>,G<sub>a</sub>) built on Poly2, which are coupled to the Poly1 gate by the capacitors between Poly1 and Poly2 denoted as C<sub>1-1</sub>,C<sub>a</sub>. Assumed with the zero initial charge on the floating-gate and only two input gates, the drain current can be written as

$$I_{D} = \frac{1}{2} \mu C_{\infty} \frac{W}{L} \left[ (k_{1} V_{01} - V_{2}) - (V_{10} - k_{2} V_{01}) \right]^{2} \quad (1)$$

$$I_{B} = \frac{1}{2} \mu C_{m} \frac{W}{L} \left[ \left( k_{i} V_{ci} + k_{j} V_{ci} \right) - V_{j} - V_{ji} \right]^{2}$$
 (2)

where  $k_1$  and  $k_2$  are capacitive coupling ratios  $C_0/C_T$  and  $C_d/C_T$  respectively and  $C_T$  is the total capacitance of the floating gate. The drain current is essentially a linear sum of all inputs weighted by the ratios. Equation (1) is arranged to show the threshold voltage tuning. It is seen that  $V_{GI}$  can be utilized as a signal port while  $V_{GI}$  is used to tune the effective threshold voltage. Equation (2) is written to show a linear sum of the weighted multiple-input voltages.

### 3. HYSTERESIS TUNABLE COMPARATOR

A hysteresis tunable comparator was proposed in [7], based on an electronically tunable positive feedback factor produced by threshold voltage tuning of the embedded FGMOS devices.

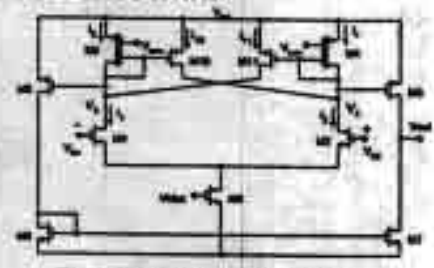


Fig.2 Hysteresis Analog Comparator

tro Mal

The hysteresis tunable analog comparator is shown in Fig. 2 where M<sub>3</sub> and M<sub>4</sub> are FGMOSs. The hysteresis involves positive feedback produced by M<sub>10</sub> and M<sub>11</sub>. The positive feedback occurs only when the current ratio of I<sub>10</sub>/I<sub>3</sub> and I<sub>01</sub>/I<sub>04</sub> are greater than one. If the ratio is higher, the amount of the feedback current will be increased and results in a wider of the positive and negative trip point voltage, V<sub>TRP</sub>, and V<sub>TRP</sub>. Hence the hysteresis can be controlled. The V<sub>TRP</sub>, and V<sub>TRP</sub>, can be derived from the condition that I<sub>2</sub> equals to I<sub>10</sub> and I<sub>4</sub> equals to I<sub>10</sub>, correspondingly as,

$$V_{IRP_+} = \sqrt{\frac{2I_3}{\beta_1}} \left( \frac{\sqrt{I_{10}/I_3} - 1}{\sqrt{1 + I_{10}/I_3}} \right)$$

$$V_{IRP_-} = \sqrt{\frac{2I_3}{\beta_1}} \left( \frac{\sqrt{I_{13}/I_4} - 1}{\sqrt{1 + I_{11}/I_4}} \right)$$
(3)

Based on (1), since FGMOS allows us to tune drain current, the ratio of loss/los and loss/los can be tuned electronically by V<sub>best</sub> at the input gate of M<sub>3</sub> and M<sub>4</sub>. Also V<sub>TRP</sub>, and V<sub>TRP</sub>, can be tuned orthogonally if the haning voltage at the input gates of M<sub>3</sub> and M<sub>4</sub> are different. M<sub>3</sub> and M<sub>4</sub> are designed with an equal area of G<sub>1</sub> and G<sub>2</sub> as 10.8×22.8µm<sup>2</sup> while the floating-gate area is set to 13.2×2.4 µm<sup>2</sup>, which is also equal to those of M<sub>10</sub> and M<sub>11</sub>. Fig.3 shows the simulation results of V<sub>TRP</sub>, and V<sub>TRP</sub>, vs. V<sub>see</sub> varied in the range of 2.5-5.0V.

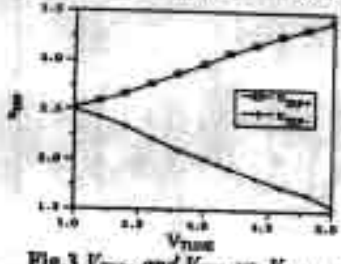


Fig.3 Vraps and Vrap. vs. Vruss

To express the performance of the comparator in a noisy environment, the circuit was tested with a noise-modulated signal with the noise amplitude set to 0.4V<sub>pet</sub>. Simulation results are shown in comparison with those from a non-hysteresis comparator in Fig. 4.

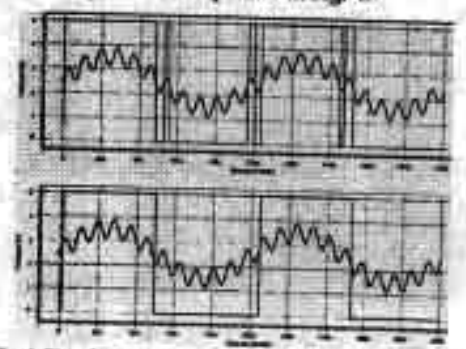


Fig.4 Simulation results without and with hysteresis

## 4. ANALOG-BASED DIGITAL COMPARATORS

Based on the proposed analog comparator, a new digital comparator [7] can be realized by doing a minor modification at the input devices. A hysteresis 4-bit digital comparators can be developed as in Fig.5 by employing FGMOSs as the input devices of which the sizes of the input gate are based on the significant of the binary weight. With hysteresis operation, this circuit performs two comparative functions of A>B or A≥B which depend on the level of V<sub>ress</sub>. It is evidently shown in Fig.3 that if V are is high or set to 5V, the current ratio losofins and IDENTON will be high and result in a large hysteresis. Then the comparator performs the operation A>B, where the value of A must be higher than B for some extent to cause the comparator tripping. On the other hand. If Vness is low or set to 0V, the positive feedback will be minimized and result in no hysteresia. Then the comparator performs the operation A≥B.

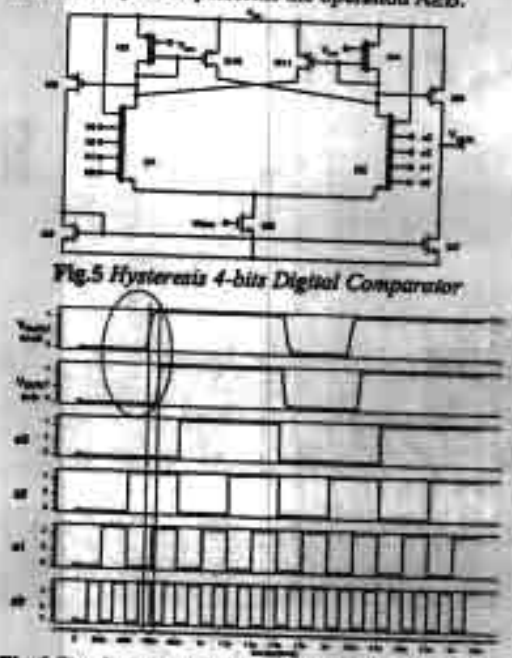


Fig.6 Simulation results of the hysteresis comparator

From Fig.6, the binary bits b3-b0 are set to \$50101 while the binary bits a3-s0 are swept digitally. It is seen that when V<sub>box</sub> is set to Low, the output signal changes its stage when both binary sets are equal. The circuit performs the function A2B. If V<sub>box</sub> is set to High, the comparator performs the function A2B. A simple non-hydresis digital comparator is shown in Fig.7 which is different from Fig.5 in that there is no positive feedback mechanism. The circuit performs three functions at the output node such as A<B, A>B and A=B. The output voltage is logic High or Low when the binary inputs at the positive terminal is higher or lower than that of the negative terminal respectively. The output is V<sub>ab</sub>/2 when the binary inputs of both terminals are equal. This particular function implies an ability to detect the equality

of the binary inputs. The functionalities are confirmed by the simulation results in Fig.8.

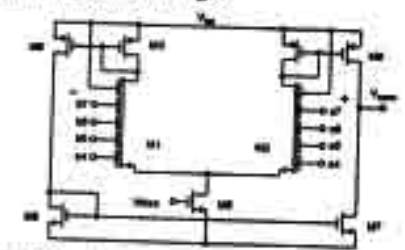


Fig.7 Non-hysteresis 4-bits Digital Comparator

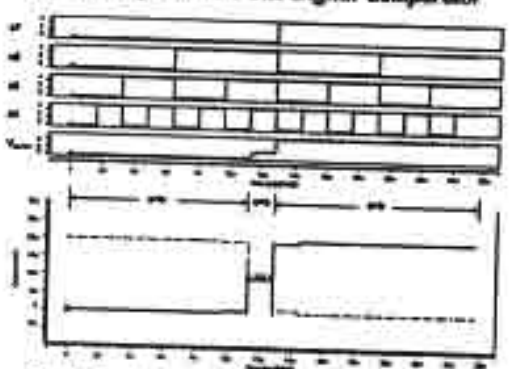
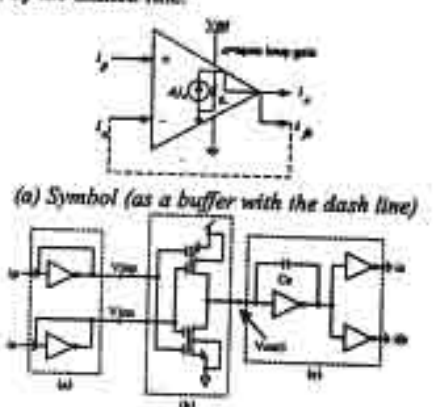


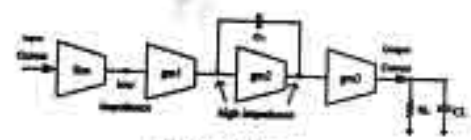
Fig.8 Simulation results of the non-hysteresis comparator

### 5. LOW VOLTAGE CURRENT AMPLIFIER

A current amplifier circuit [8] totally formed in the class AB structure utilizing CMOS inverters and FGMOS devices is presented here on 0.5µm double poly CMOS processes with 1.5V. As a buffer, the amplifier can deal with wide signal swings up to ±200µA, with 1% of the THD and 10pF of C<sub>L</sub>. The proposed current amplifier, as symbolically shown in Fig.9(a), has two identical input terminals denoted as i<sub>p</sub> and i<sub>n</sub> and two output terminals delivering the same phase of the signal denoted as i<sub>p</sub> and i<sub>n</sub>, which are used as the output and the feedback port respectively. It is noted that the input i<sub>n</sub> can only be symbolized as an inverting terminal when the amplifier is connected in the negative feedback configuration as shown by the dashed line.



(b) The proposed current amplifier



(c) Block diagram
Fig.9 The proposed current amplifier

In Fig.9(b), the amplifier comprises three circuit blocks as shown in the dashed boxes. The transimpedance amplifier is shown in box (a) and written as

$$Rm = \frac{1}{(gm_e + gm_p)}$$
(4)

D

where gm, and gm, are respectively the transconductance of NMOS and PMOS of the inverter. The additive analog inverter in box (b) is basically a two-input CMOS inverter elegantly built from the floating-gate MOSFETs and proposed in [9]. It is employed in this circuit together with the other Rm blocks to work as a differential amplifier. Hence the polarity of it is inverse to those of it, causing the voltage at node V<sub>ina</sub> to be inverse to those at node V<sub>inp</sub>. Based on the diagram in Fig.9(c), the open-loop current gain of the whole circuit can be derived as

$$A_i = Rm \cdot gm_i r_{ei} gm_2 r_{e2} gm_3 \tag{5}$$

where rel, reg are the output resistance of gm1, gm2 stages while the GBW is

$$GBW = \frac{Rm \cdot gm_1gm_1}{C_C}$$
(6)

The final design schematic can be illustrated in Fig.10, where it is seen that the circuit can be designed in a modular fashion where all inverters including the additive analog inverter have the same dimensions of NMOS and PMOS correspondingly. If a higher gain of the gm<sub>2</sub> and gm<sub>3</sub> blocks is required, we simply add more cells of the identical inverters in parallel. R<sub>C</sub> and C<sub>C</sub> are employed for the frequency compensation.

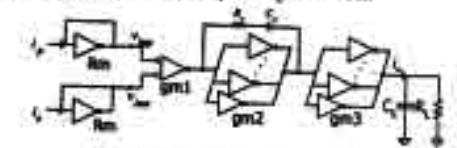


Fig.10 Design schematic

On the Alcatel 0.5 $\mu$ m CMOS process, the amplifiers have been designed with  $V_{0D}$  of 1.5V. All NMOS and PMOS are designed with the dimensions of 6.9 $\rho$ 0.5 and 23.6 $\rho$ 0.5 respectively resulting in the idle currents of 30 $\mu$ A for each inverter. Four and three inverters connected in parallel are employed for the gm<sub>1</sub> block and the gm<sub>2</sub> block respectively to increase the gain. The amplifier is loaded with  $C_L$  of 10 $\rho$ F and  $R_L$  of 1.69 $\mu$ C, while  $R_C$  of 1 $\mu$ C and  $R_L$  of 0.8 $\mu$ F are set in the compensation scheme. The circuit was simulated on HSPICE with the performances shown in Fig.11 where 69.6dB Open-loop gain, 127MHz GBW and 74 $\rho$ PM were achieved with 635 $\mu$ W power consumption.

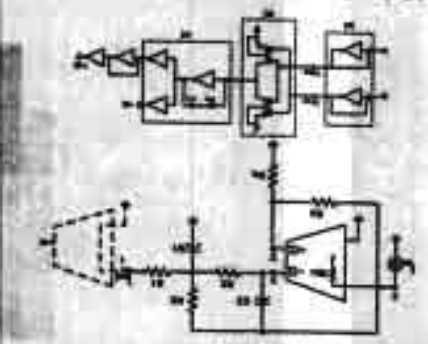
Simulation results   Ideal care calculations			Design peramoters						
me.I	une on	esc.)	DC gain	(CHO,PA	(CDOPH	Ratha	Cathr)	(40)P)	(2)-104
(2549)	(90)	(23-8%)	(90)	DOR F	818.0	2,459	00	160	
121	010'0	21.12	901.0	609.F	818.0	2,459	09	- 08	
797	010.0	334	601,0				202	25	
3.90	1-08.0-	334	0.540	1991	806.0	22972		40	
60.8	010.0	35.5	901.0	606/1	8190	869°Z	50		
TE.8	010.0	71.2	0.109	609.1	6190	2,459	- OL	25	_
08.7	155.0-	50.8	091'0	1,651	0.840	2252	EL.	92	- 6
6.90	6000	58.8	991.0	572.	1990	3,555	11	22	7
	010.0	£8.7	601.0	909.1	613.0	2.459	04	30	
10.2	0.004	36.8	660.0	068.1	508.0	2,429		18	6
121	010.0	E0.6	601.0	909.1	0.819	2.459	8	91	OL.

raple i Design parameters and simulation re

oth toll s2OMOH to memocalqui gnizzi solanaquios leligib hysteresis-tunable analog comparator. Consequently, the proposed analog comparator circuit is developed to a comparators which exploit the threshold voltage operation characteristic of PGMOS to produce a We have reviewed the designs of analog and digital

### e. CONCLUSIONS

Fig.12 Single-ended input dual-feedback Bigund



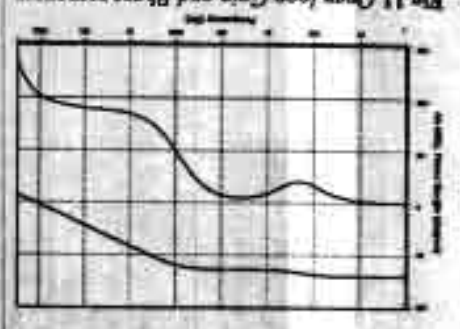
agreement with the ideal case.

Table 1. It is seen that the simulation results show a good shown in Fig.13 and in comparison with an ideal case in which correspond to the design parameters of  $R_a$   $R_b$ ,  $C_b$ ,  $R_b$ ,  $R_d$  and  $R_b$  for various cut-off frequencies in the range of 1-10 MHz in Table 1. The simulation results are

$$f^{-90} = 5MH^2 \ \tilde{O}^0 = 1 \ H^0 = 1$$
 (2)

design example, we assume filter specifications sa, with dual feedback in Fig.12 [10-11]. To demonstrate a on the general single amplifier network configuration current amplifier is demonstrated as an application, besed A current-mode filter implementation using the

Fig.11 Open loop Gain and Phase responses



[13] T. Shiban, T. Ohmi, "A Fluccional MOS Translator Featuring Onto-Level Weighted Sum and Threshold Operations", IEEE Trans. Six. Devices, vol. 24, 1992, pp. 1664-1655.
[23] J. R. Angulo, G. Oonzalez-Altamirane, S.C. Choi, "Adodeling municiple-input floating-gast transminar his analog rights processing," ISCASSY, Vol. 3, pp. 2020-2023.
[24] Libring Yin, S. H. K. Embald, E. Sanchez-Stansnick, "A Sonting-part factoring-gast devices: Toylouing-part for analog and transmission," A Sonting-level of the Constant, "Hearing-gast devices: Toylouing-gast devic 7. REFERENCES

(11) G.S. Mosekyar, A. Curkones, "A. Cleanficstion of Current-Mode Single-Ampilier Biquada Based on a Voltage-to-Current Transformation", IEEE Trust. Co. CAS, Vol.4), no. 2, pp. 151-156

13] A. Venavelli, E. Sancier-Simmolo, J. Silva-Martinez, Transconductances muplifier structures with very musti-seminorductances amplifier structures with very musti-seminorductances a comparative design approach. J. Solid-State Clerulit, Vol. 37, Jenne 11 May 1003, pp. 500-532

[6] K. Mandhard, I. Mgammel, K. Moodpho, "A 2,8V RWDM BTL 19CAS2002, Vol. 5, pp. 261-264

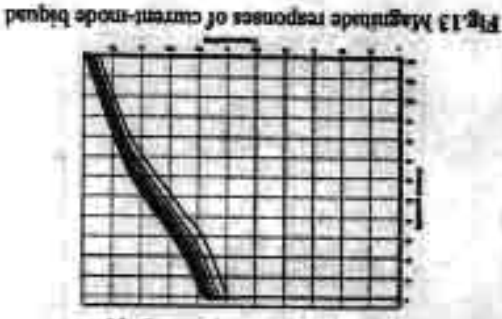
[7] K. Mondhard, I. Mgammel, R. Moodpho, "A 2,8V RWDM BTL 19CAS2002, Vol. 5, pp. 261-264

[8] K. Moodpho, J. Mgammel, R. Mendhard, "A low-voltage vide comparation with FGMOS current supplifier," IBCAS2002, Vol. 4, pp. 559-662

[9] Y. Borg, O. Messen, M. Hovit, "Ultra hav voltage floating-gate requirements are printed for voltage floating-gate for the processing structures amplifier, "A flower printed for the processing floating-gate floating-floating-gate floating-floating-gate floating-gate floating-gate floating-gate floating-gate floating-gate flowers flow to the processing floating-gate floating-gate flowers flowers flow video frequencies". HEE froc.-Circuita between Sym. vol. 147, No. 1, 2000, pp. 35-41.

[10] M. Schmid, G. Schonder, "Antivo-MOSFIT-C angle-surplifier between Sym. vol. 147, No. 1, 2000, pp. 35-41.

[10] M. Schmid, G. Schonder, "Characteria". HEE froc.-Circuita between Sym. vol. 147, No. 1, 2000, pp. 35-41.



for low voltage and electronically tuning applications. functionalities. It is seen that FOMOS is a unchil device of the weighted multiple-input binaties. Design and application of the low voltage current-mode amplifier using inverters and FOMOSs are also presented. input devices of which the drain currents are linear surns

[5] K. Moolpho, J. Ngarmnil, S. Sitjongsatapom, "A high speed low input current low voltage CMOS current comparator", 2003 IEEE International Symposium on Circuits and Systems (ISCAS2003), Bangkok, May, 2003.

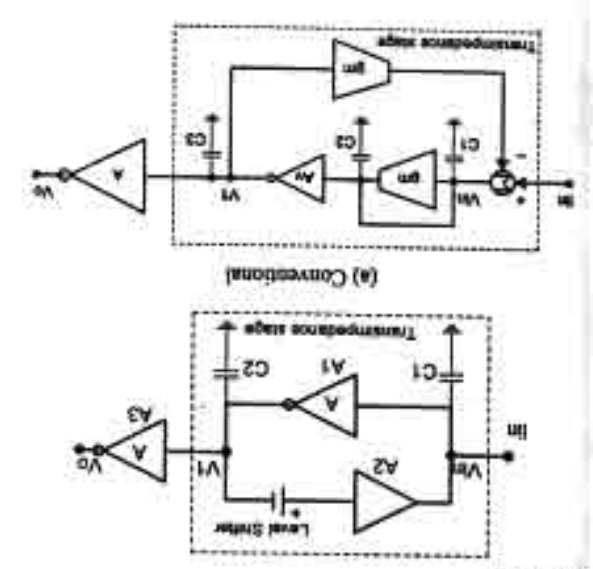
## A High Speed Low Input Current Low Voltage CMOS

## Current Comparator

K. Moolpho, J. Mgarmail, S. Sitjongsataporn

Electronic Engineering Department
Mahanakorn University of Technology, Bangkok, Thailand, 10530
Email: jitkasam@mut.ac.th

only CMOS inverters and is suitable for a low Vpp to the latter high gain inverter amplifier. The circuit utilizes lower sain is emphasized to gain speed and then trade power propose an idea based on Figure 1(b), where a much higher to provide the rail to rail output swing. In this paper, we high gain of the latter inverter amplifier will be necessary voltage swing of the tramesistance stage is desired, a very thems a to thuser a sa beeds a it radi tollinoo a ai ersult high with hence a higher power consumption. Obviously, the gain of the latter inverter amplifier must be necessarily drawback of having the small voltage swing at V, is that comparators are insensitive is then minimized. However, a which is the smallest input current range to which current in the pico Amps range. The so called dead zone could be much lower and receive a much smaller input with a larger loop gain, the input impedance at node V., keep the signal Vis and Vi as low as possible. Moreover to betriofer need for sail has not been exploited to the transimpodance stage is formed in a negative feedback create Vos of the buffer MOSFETs. It is seen that although utilized diode connected MOSFETs as a level shifter to



(b) Proposed
Figure I Current comparator concepts

### ABSTRACT

A new high speed low input current comparator is proposed in this paper. Based on a simple negative feedback scheme around the transimpedance stage with an emphasis on a very large loop-gain, the transformed voltage signal is maintained at the lowest awing that tesults in a speed improvement. On a 0.25mm TSMC CMOS process, simulation results demonstrate propagation delays of 3.6ns with ±100nA input current and 1.5Volts power of 3.6ns with ±100nA input current and 1.5Volts power supply, while the smallest input current is ±50pA.

Performances are also shown with other Vap such as 1.0,

### I. INTRODUCTION

MOSTETS of the buffer As all the time. Most of them ability by arranging a proper biasing to turn on the were relating to improve the lowest input current acquiring voltage of the inverter A. However, the reported works possible and situated exactly around the inverter threshold the signal swing at V, should be maintained as armall as produce output logic voltage. There exist parasitic capacitors at all nodes, Ideally for high speed comparators, on the latter high gain inverter amplifiers As to voltage buffer A<sub>2</sub>. The resulting voltage V<sub>1</sub> is then transimpedance stage comprising invertor amplifier A<sub>1</sub> and signal is converted to the voltage Va and V, by the block diagram in Figure 1(a), where the input current comparators [4]-[7] are based on the concept shown as a propagation delay. Conventionally, most reported current voltage swing carefully since it directly determines the speed current comparator, one has to take care of the current to a large voltage signal. Thus to design a high Obviously there is a requirement to transform the input Jangia agastov tian or tant to reigol langib si langia suquo operation since although the input signal is current the key elements. The circuit is not purely in a current-mode signal processing, the current comparator is also one of the node voltages swing are very low. In analogue and mixed operation, all of which are mainly due to the fact that all such as high speed, wide dynamic ranges and low voltage sensory systems. This is due to their attractive features bes attentia batergatui mabom tol tenatni lo stol nwanb In the last decade, current-mode circuits [1]-[3] have

### 2. THE PROPOSED CIRCUIT

As discussed above, we concentrate on a high speed or smallest average propagation delays and low input current acquiring capability or smallest dead zone, in this work, we trade off power for the required speed by maintaining the lowest voltage swing of the transimpedance stage and then providing high power to build up the latter high gain stage using inverter amplifiers. We then focus on the two separated circuit blocks as follows.

### 2.1 TRANSIMPEDANCE STAGE

VinutO.25um for W/L of NMOS and PMOS respectively. ben ame dimensions which are 2.1 una C. Sum and amplifiers A<sub>1</sub> to A<sub>4</sub> are CMOS inverters designed with the provide negative feedback current to the input node. All respectively. The transconductance amplifier A. is used to from a parasitic capacitor and a triode MOSPET set to 1.6k Ohms. Note that the C and R could be made stable. Capacitor C is set to 0.1pF while the resistor R is frequency compensation is necessary to make the circuit Diff qool soft in readon somebaquit figid own are stack amplifiers constructed from two casesded invertors. Since the value of Lign. As and As are two high voltage gain inverter is basically an equivalent grounded resistor with A as a shorted input-output transconductance amplifier or polarities of output voltages and currents of each invarier. formed in a negative feedback loop by observing the speed of the comparator, it is seen that the whole stage is Figure 2, plays the most important role in determining the The transimpedance stage, shown as the dashed block in

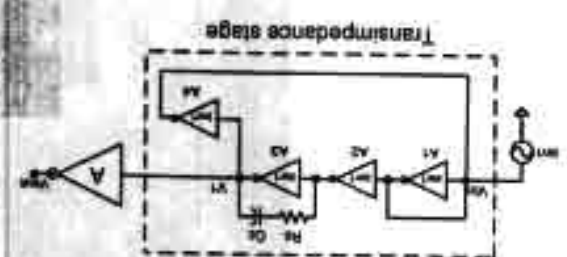


Figure 2 Transimpodance stage

Constructed in the feedback loop, the input resistance at node V<sub>in</sub> can be derived as.

$$R_{in} = \frac{1}{8m_T} \frac{1}{(1 + A_L^2)}$$
 (1)

where gm<sub>1</sub> is an equivalent transconductance of A<sub>1</sub> and A<sub>2</sub>. Note and A<sub>2</sub>, is a voltage gain of the amplifier A<sub>2</sub> and A<sub>2</sub>. Note that all inverters have the same transconductance and voltage gain because they have the same dimensions. It is seen that the input resistance H<sub>2</sub>, is very small which results in a minimum voltage awing at node V<sub>2</sub> and also results in a minimum voltage awing at node V<sub>2</sub>, and also results in a minimum voltage awing at node V<sub>3</sub> and also the same value of V<sub>1</sub> at the output of A<sub>2</sub>. Figure 3 shows an

open loop gain and phase of the feedback current to the imput current. It is seen that de gain of 56dB, GBW of 906MHz and PM of 45° are achieved in the open loop transconductance stage. With this specification, we have coough loop gain to suppress signals for the lowest voltage savings at V<sub>in</sub> and V<sub>i</sub> as shown in Pigure 4. The negative feedback also stabilizes the common-mode voltage at all nodes to V<sub>DO</sub>2 which is set by the node V<sub>in</sub>. This property is crucial for assuring that the signal swing is very small is crucial for assuring that the center of the gate threshold and also situated right at the center of the gate threshold

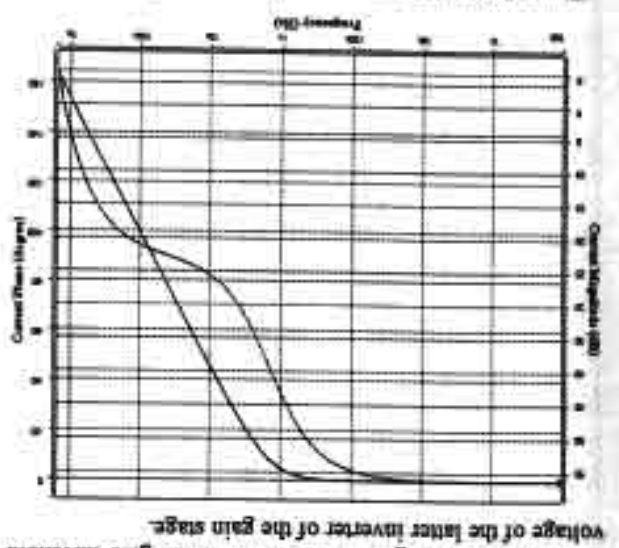


Figure 3 Open-loop responses of the transconductance stage

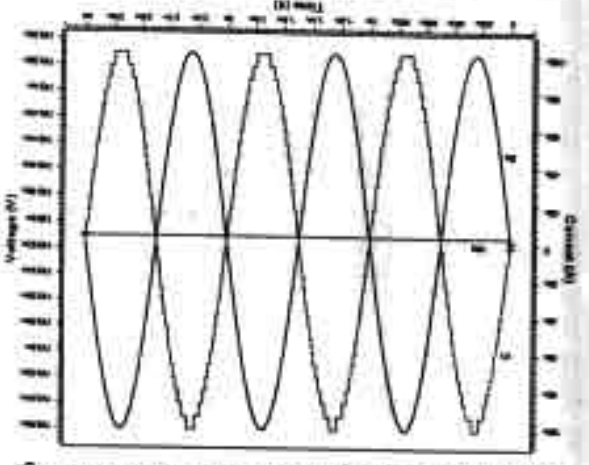


Figure 4 Voltage swings at Va and V, vs. input current

2.2 GAIN STAGES

We have now a very small voltage awing V<sub>1</sub> at the input of A<sub>5</sub> of the gain stage. The main aim in designing this part is to construct high voltage gain to produce rail to rail output logic. Based on the use of the same dimension inverters, we can construct the high gain stage in a modular fashion. INVI has the same dimension as those in the

transconductance stage. INV2 has amaller dimensions than those of INV1 by half, i.e. 1um/0.25um and 3.5um/0.25um for W/L of NMOS and PMOS respectively. The modules could be placed in parallel for higher gain. For A<sub>5</sub>, there are six INV1s connected in parallel, where each INV1 possesses an output current equal to I<sub>in</sub>. A<sub>5</sub> and A<sub>16</sub> are only needed when I<sub>in</sub> is lower than 10nA. Cascading many stages of the inverter does not deteriorate the speed much because each inverter has a very small propagation delay which is less than 1 ns. So as discussed earlier the major contributor to the delay is the transimpedance stage.

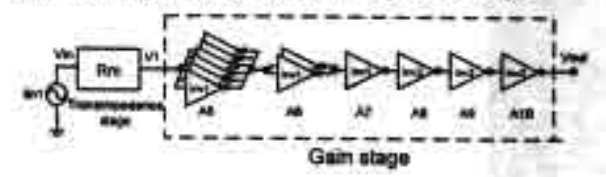


Figure 3 Gain stage

### 3. SIMULATION RESULTS

The proposed current comparator has been designed on a 0.25um TSMC CMOS process and tested with various power supplies and input current amplitudes. On HSPICE and with Vpp set to 1.5V, the comparator responses of three input current amplitudes of IuA, 100nA and 100pA are shown in Figure 5 where the average propagation delays are 1.95ns, 3.6ns and 10.7ns respectively. Performances vs the input current amplitudes at 1.5V Vpp such as average propagation delay, static power and power delay product (PDP) are shown in Figure 6. It is seen that the lowest input current amplitude is at ±50pA thanks to the small input resistance as a result of the negative feedback with high loop gain. The average propagation delay is inversely proportional to the input current amplitudes since the voltage swing at the output of the transconductance stage is small. With small input current amplitudes, the static power also increases because all node voltages are around the common-mode value or V<sub>DD</sub>/2 where most MOSFETs of the inverters are fully turned on Propagation delays at various Vop and imput signal amplitudes are shown in Figure 7. Performance comparisons among many reported circuits are listed in Table 1. It is seen that the power is higher than those from some earlier designs because the scaling down of the Vpo normally degrades some properties of the inverter such as average drain current, voltage gain and propagation delay. Thus more power has to be pumped into the circuits in order to achieve the required speed and rail to rail output voltage swing.

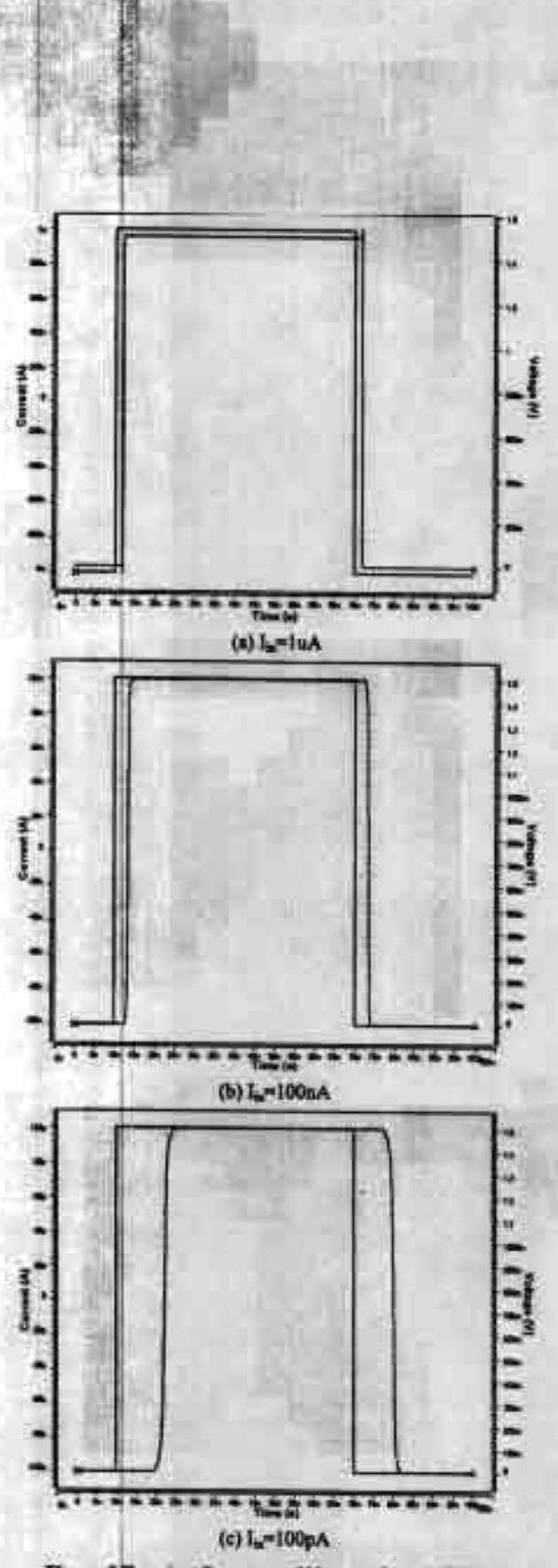
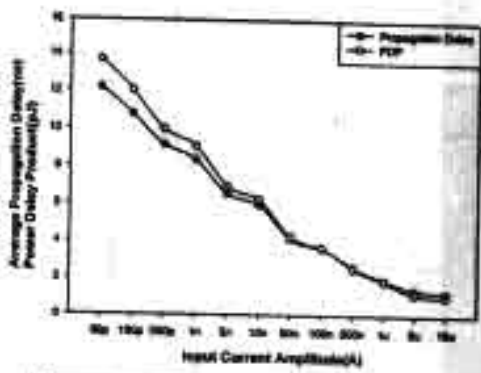


Figure 5 Transient Response of Voor vs. Is at 1.5V Voo



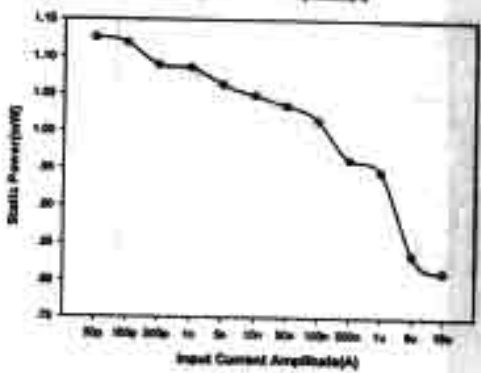


Figure 6 Performances at 1.5V Von

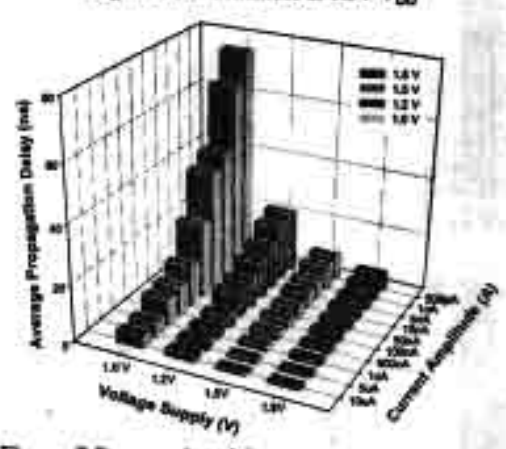


Figure 7 Propagation delays at V<sub>DO</sub> 1.0-1.8 Volts

### 4. SUMMARY

A new high speed low input current low voltage current comparator has been demonstrated on a 0.25um TSMC CMOS process. Based on the concept of a high speed current-mode technique, we exploit a negative feedback scheme around the transimpedance stage with an emphasis on a very large loop-gain to produce a very small transformed voltage swing which is situated at the center of the gate threshold voltage of the latter stage. This will ensure the fastest response time. The same dimension inverters are used in all amplifier stages. They are fast and simple and suitable for low voltage operation. There is no extra biasing circuit and stacked transistor, thus the same design can be applied with various VDO - ie there is no need to readjust the design.

### 5. REFERENCES

[1] C. Tournazou, F.J. Lidgey, D. Haigh, "Analogue IC Design:

The current-mode Approach", Peregrinus, UK, 1990.

[2] G. Palmisano, S. Pennisi, "Low-Voltage continuous-time CMOS current amplifier with dynamic biasing". Proc. ISCAS2001, Sydney, May 2001, pp. 1-312-1-315.

[3] K. Moolpho, J. Ngarmnil, K. Nandhasri, "A low-voltage processing Processi

wide-swing FGMOS current amplifier", Proc. ISC452802, Phoenix, May, 2002, pp.713-716.

[4] H. Traff, "Novel approacch to high speed CMOS current companiors", Electronics Letters, Vol.28, No.3, pp.310-312,

[5] A.T.K. Tang and C. Toumazou, "High performance CMOS current comparator", Electronics Letters, Vol.30, No.1, pp.5-

[6] L.Ravezzi, D.Stoppas and G.F. Dalta Betta, "Simple highspeed CMOS surrent comparator", Electronics Letters, Vol.33, No.22, pp.1829-1830, 1997.

[7] H. Lin, J.H. Huang and S.C. Wong, "A simple high-speed low current comparator", IEEE Trans. Circuit Syst., pp.713-716, 2000.

[8] B.M. Min and S.W. Kim, "High performance CMOS current comparator using resistive feedback network", Electronics Letters, Vol.34, No.22, pp.2074-2076, 1998.

ACKNOWLEDGEMENT This work has been supported by a grant from the Thailand Research Fund (TRF).

		Table 1	Performance co	muurisees			_	-
	Traff[4]	Tang [5]	Raverri[6]		Lin [7]	Proposed circuit		
Year	1992	1994	1997	1996	2000	2002 2002		
Power Supply (V)	5	5	5	1	- C (2	14	1.0	2002
Process (jum)	2	1.6	2.5	0.35	0.35	0.34		1.8
Minimum Input Current Amplitude (nA)	10	10	100	10	1	0.25	0.25	0.25
Propagation dalay	±1jaA/ 10na	±0.1µA/	±0.1µA/	±0.1µA/ 7ms	±6.tpA/	±0.1µA/ 3.5ms	±0.1µA/	±0.1µA
Power consumption (mW) (at 0.1µA)	0.390	1.4	NA	0.45	0.58	1.01	0.022	2.6ms 2.73
PDP (pJ)	NA.	NA	NA	3.15	14	3.648	0.32	7.25

[6] J. Ngarmnil, S. Ruengrungson and K. Nandhasri, 'A 100MHz ±0.75V FLOATING-GATE MOSFET CURRENT CONVEYOR', 2003 IEEE Midwest Symposium on Circuits and Systems (MWSCAS2003), Cairo, December, 2003.

# A 100MHz ±0.75V Floating-gate MOSFET Current Conveyor

J. Ngarmnil, S. Ruengrungson and K. Nandhasri

Department of Electronic Engineering, Faculty of Engineering, Mahanakorn University of Technology, Bangkok 10530, Thailand Email: jitkasam@mut.ac.th

Abstract-This paper proposes a low voltage inverting second tration current conveyor working up to a 100MHz with 5V power supply. The circuit is formed in class AB structure g CMOS inverters and a pseudo floating-gate MOSFETs tive analog inverter facilitating a negative feedback loop to linte accurate signal tracking of the terminal voltage X to Y the terminal current Z to X. Simulation results on 0.5µm ble poly CMOS processes confirm high precision conveying area, wide signal swing and low voltage capabilities of the ent conveyor.

### I. INTRODUCTION

Recently, several signal processing techniques [1-2] id on second generation current conveyors (CCII) have a demonstrated successfully such as filtering, log-domain slinear, squarer and rectifier and multiplier circuits. Most eted CCII structures are based on a translinear cell which acked on current mirror circuits. A high precision CMOS I [3] was also realized with voltage follower and current ors with an emphasis on local negative feedback loop ind v, and v, terminals. All these circuits have suntered with limitation on low voltage applications since circuits are based on stacking topology of transistors. For voltage applications, a CMOS CCII [4] was proposed ly using CMOS inverters allowing only two stacked ces between the supply rails. The circuit is in a class-AB of which the current signal swing can be very high suse there is not any fixed bias current source to limit the al swing. However, the circuit is restricted to applications re the Y input is only referenced to signal ground. A sed voltage follower based CCII was also proposed ntly in [5] exhibiting performances on low voltage and pactness. However, the current signal swing of terminal X Z are limited to the fix bias current source.

In this paper, we proposes a new inverting second eration current conveyor 'positive' (ICCII+) totally ted in the class AB structure utilizing CMOS inverters and recently proposed additive analog inverter [6-7] using ido or Quasi floating-gate MOSFETs, of which the offset age of the floating gate terminal can be weakly controlled ctively via a large valued resistor thanks to the inventions cosed in [8-11]. The design is emphasized on negative back with a high loop gain to enhance the conveying issions relating to v<sub>y</sub> to v<sub>x</sub> and i<sub>x</sub> to i<sub>x</sub>. Thanks to the class

AB topology, the circuit is also capable with wide swing signals. The design is applied on a 0.5 µm double poly CMOS with ±0.75V power supply demonstrating low voltage capability and high frequency operation up to 100MHz.

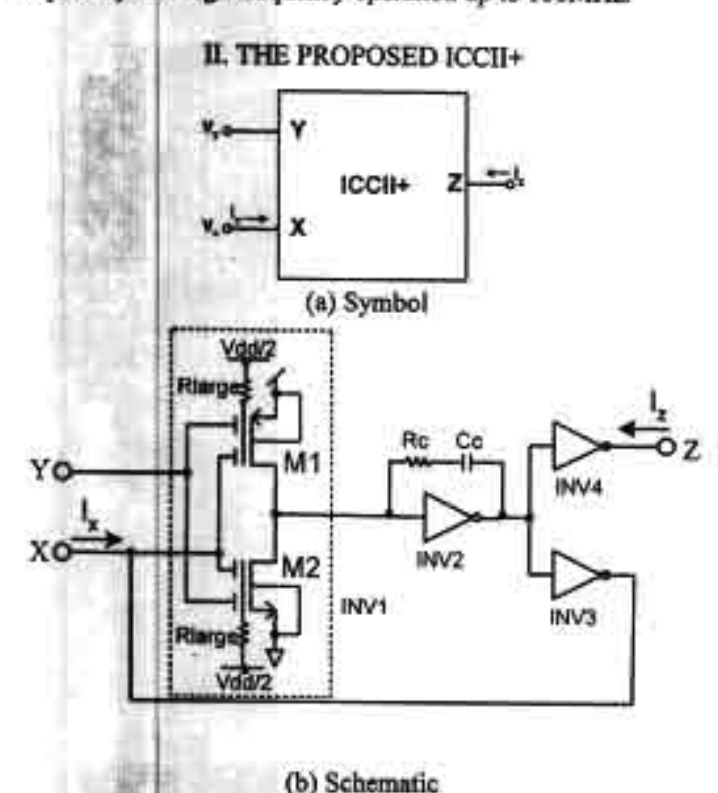


Fig.1 The proposed ICCII+

The proposed ICCII+ is shown in Fig.1 of which the port relations [12] among voltage and current terminals are described as

$$\begin{bmatrix} i_y \\ v_z \\ i_z \end{bmatrix} = \begin{bmatrix} 0 & 0 & 0 \\ -1 & 0 & 0 \\ 0 & 1 & 0 \end{bmatrix} \begin{bmatrix} v_y \\ i_z \\ v_z \end{bmatrix}$$
(1)

where terminal Y is a high impedance node and does not draw any input current. Terminal X is a low impedance node with voltage value  $v_x$  equal to  $-v_y$ . Terminal Z is a high impedance node with the terminal current  $i_x$  equal to  $i_x$ . These properties are transformed to the proposed ICCII+ shown in Fig. 1. It is n that Y is connected to the input gate of floating-gate ISFETs and is perfectly a high impedance node. Z is nected to the output node of an inverter which is obviously igh impedance node with current driving capability. It will shown later on that there is an internal negative feedback p from Y terminal to X terminal. By virtue of the negative floack loop, X can be derived as a low impedance node a current driving capability by inverter INV3 which is wn in Fig.1(b).

In Fig.1(b), the ICCII+ comprises four circuit blocks ignated as INV1, INV2, INV3 and INV4. The INV1 is an itive analog inverter or basically a two-input CMOS erter built from floating-gate MOSFETs M1 and M2 and proposed in [6-7]. Based on the idea of Pseudo or Quasi ting-gate MOSFET in [9-11], large value resistors trge) are shown to connect the floating-gate terminals of and M2 to Vdd/2 thus the DC offset of the floating-gate SFETs can be effectively controlled and the complicated al charge programming scheme such as UV removal can avoided. The resistors are built from reverse-biased diode nected PMOSs. The INV1 is employed in this circuit ther with INV2 and INV3 blocks to mimic the function of erential amplifier which allows the output of INV3 to atively feedback to the node X. Since voltage polarity of /3 output is inversed to those of v<sub>y</sub> causing the voltage at e vx to be inversed to those at node vx hence the function averting CCII to copy the voltage -v, to v, can be fulfilled. reover, the diode connected PMOSs are always in reverse because voltage at the floating-gate is small as a result of negative feedback. A modulated AC voltage at the ting-gate can be written in (2) where the coefficient of v egative as a result of the negative feedback via INV2 and 13.

$$v_{PG} = k_1 v_y - k_2 |v_z| \qquad (2)$$

e k1 and k2 are the capacitive division factors C<sub>1</sub>/C<sub>T</sub> and C<sub>2</sub>, where C<sub>1</sub> and C<sub>2</sub> are the input coupling capacitances of and M2. C<sub>T</sub> is the total capacitance seen from the floating. All capacitances correspond directly to the sizes of the it coupled gates. In this case, the equal input coupling C<sub>1</sub> C<sub>2</sub> of M1 and M2 are set to 60fF and 100fF respectively result in approximated equal values k<sub>1</sub> and k<sub>2</sub> of 0.5. A Il signal voltage gain between the output V<sub>est,INV1</sub> and the trential inputs can be derived as

$$\frac{\partial V_{out,DW1}}{\partial (V_y - V_z)} = -(gm_{1x} + gm_{1p})(r_{oln} // r_{olp})$$
(3)

re  $gm_{la}$ ,  $gm_{lp}$  and  $r_{ola}$ ,  $r_{olp}$  are the respective sconductance and output resistances of M1 and M2 sectively. The voltage transfer of  $v_p$  to  $v_n$  is derived as

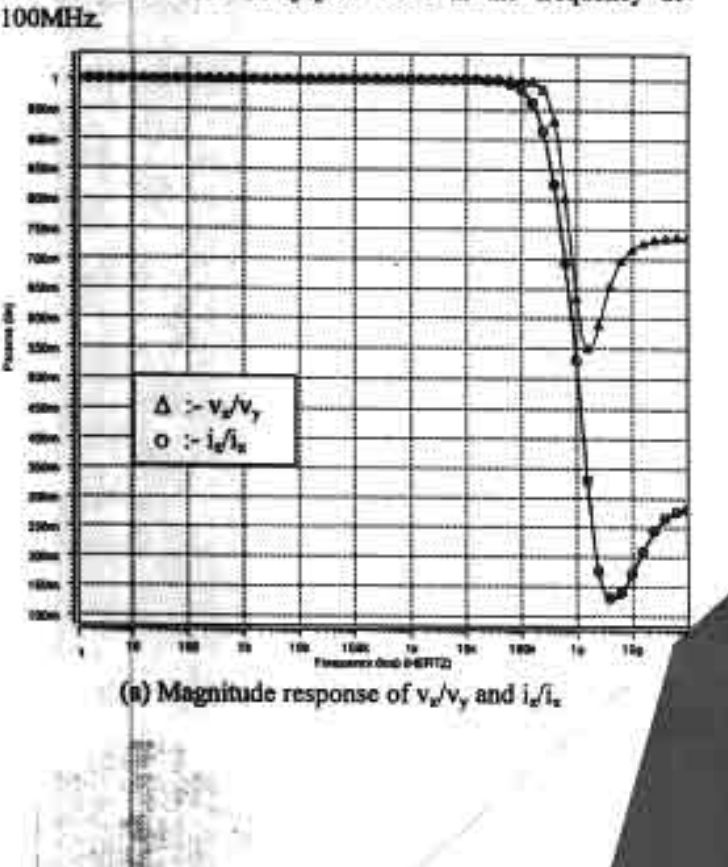
$$\frac{v_s}{v_s} = \frac{-gm_1r_{o1}gm_2r_{o2}gm_3r_{o3}}{1 + gm_1r_{o1}gm_2r_{o2}gm_3r_{o3}} \approx -1$$
 (4)

where  $gm_1r_{b1}$ ,  $gm_2r_{b2}$ ,  $gm_3r_{b3}$  are the intrinsic voltage gain of the INV1, INV2 and INV3 respectively. We can also derive the output resistance of terminal X as  $r_x$  in (5) which is low as a result of the negative feedback.

$$\frac{1}{1 + gm_1r_{o1}gm_2r_{o2}gm_3r_{o3}}$$
 (5)

### III. SIMULATION RESULTS

Based on the proposed schematic in Fig.1(b), the circuit can be designed in a modular fashion where all inverters including the additive analog inverter have the same dimensions of NMOS and PMOS correspondingly. If a higher gain of any inverter blocks is required, we simply add more cells of the identical inverters in parallel. The circuit has been designed on the Alcatel 0.5µm double poly CMOS process with ±0.75V power supply. For each inverter module, NMOS and PMOS are designed with the dimensions of 8.4/0.5 and 24/0.5 respectively corresponding to gma of 344uA/V and gm, of 314uA/V and resulting in the idle currents of 34uA for each inverter. The compensation network with Rc of 500 Ohms and Cc of 0.35pF are employed for stability since there are two high impedance nodes across INV2. In this circuit, we employ only one CMOS inverter for the additive inverter INV1 block. There are nine inverters connected in parallel for INV2 and three parallel inverters for INV3 and INV4 blocks hence making it equals to it. Both X and Z terminals are loaded with external resistors of 1kΩ. Fig.2 shows frequency responses of the ratio v./v, and i./i. which are seen that the circuit contributes very low tracking errors of va/vy to less than 1% and those of i/i, to 1.6% at the frequency of 100MHz.



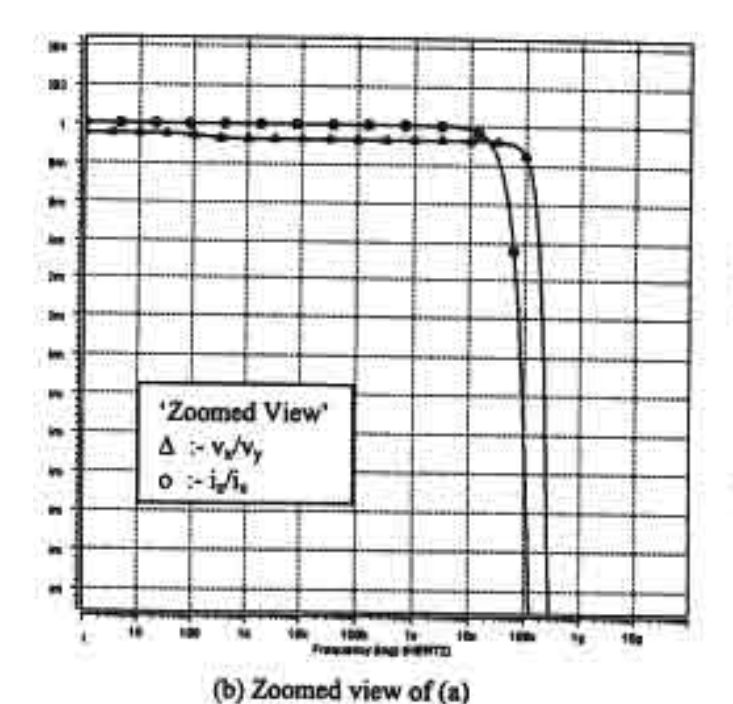


Fig.2 Magnitude responses of v<sub>s</sub>/v<sub>y</sub> and i<sub>s</sub>/i<sub>x</sub>

The magnitude responses of the X terminal output tance r, was derived in (5) and is shown in Fig.3. The e is less than 1 Ohms at DC rising to 500 Ohms at vIHz. It is increasing dependent to the frequency in the frequency range because the loop gain of the negative back is decreasing at high frequency. However, the ating frequency of the circuit is bound to 100MHz.

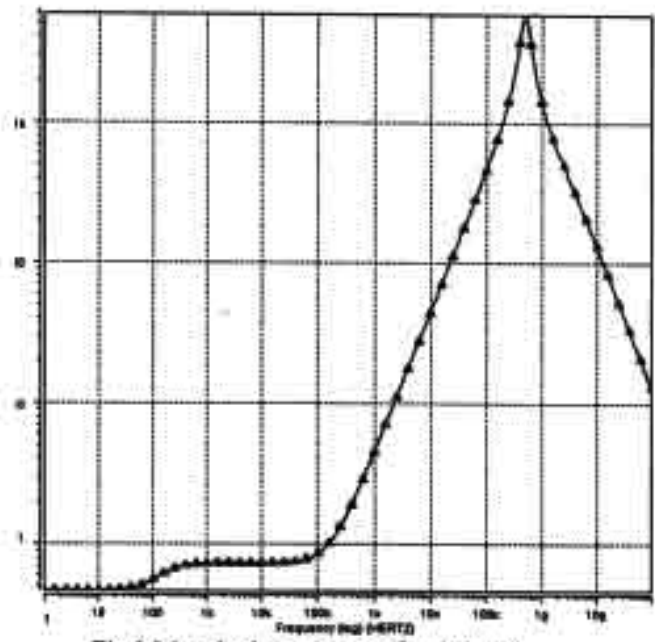


Fig.3 Magnitude response of rx (Ohms)

I shows the transient responses at 10MHz of v<sub>y</sub> vs. v<sub>s</sub> and i. i<sub>s</sub>. In Fig.4(a) the responses of v<sub>y</sub> vs. v<sub>s</sub> confirm well (4). It is seen that the signal swing is as large as lmV. Fig.4(b) shows a perfect matching of i<sub>s</sub> vs. i<sub>s</sub> with

the current swing as large as ±500uA. For high frequency capability, Fig.5 shows the transient responses at 100MHz. In Fig.5(a) shows the responses of v, vs. v, with signal swing of ±200mV. Fig.5(b) shows the responses of i, vs. i, with the current swing of ±200uA. It is seen that the corresponding signals v, vs. v, and i, vs. i, are still matched but with a small phase shift. All signal amplitudes are set to confine the THD to less than 1%. Total power consumption is 816µW which can be lowered with a reduced bandwidth.

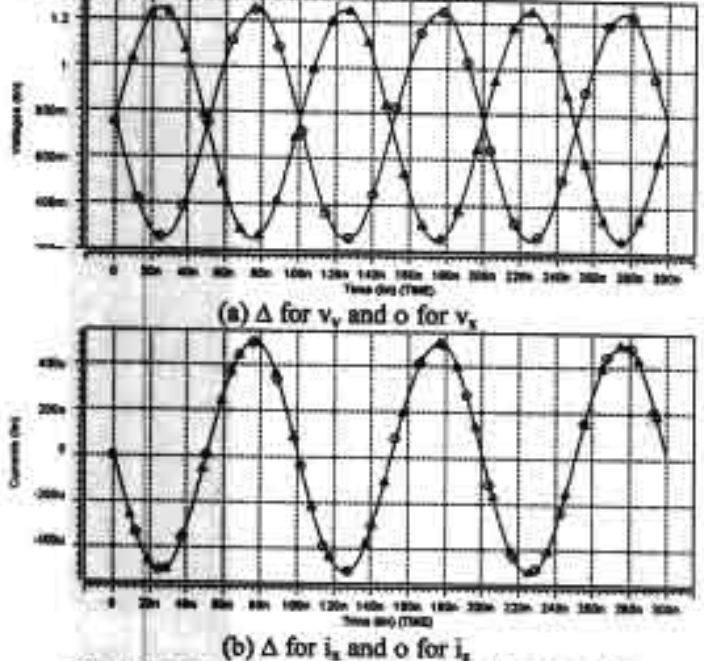


Fig.4 Transient responses at 10MHz with THD<1%

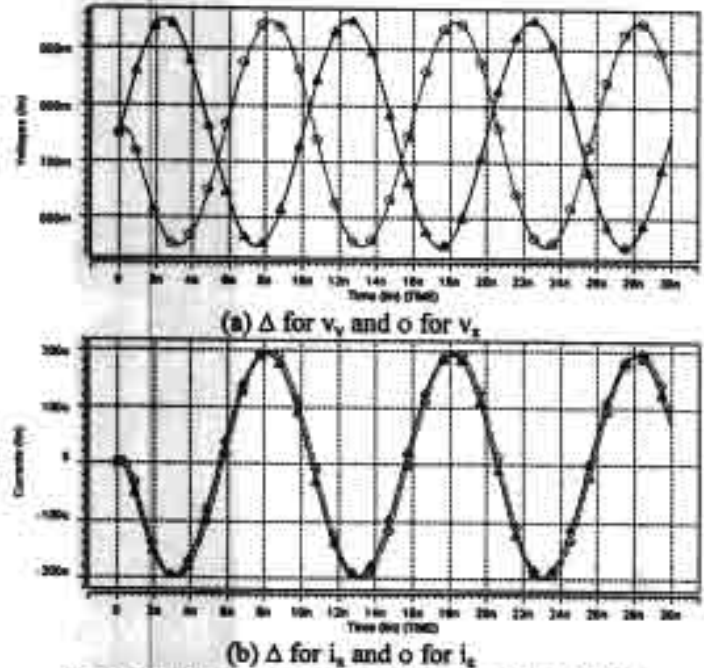


Fig.5 Transient responses at 100MHz with THD<1%

In many current conveyor applications, there is a need to have both polarities of output current iz or multiple outputs iz. and iz. In some conventional CCII, this facility is usually

formed using additional current mirrors to copy and invert srity of the output current iz. However non-ideal racteristics of current mirror always introduce some king error between the current iz, and iz. In the similar on this topology, we can not straightforwardly cascade itional inverters at the output Z terminal in order to make inverted-direction current iz, since there is usually an ess phase shift that causing an unperfected tracking ween the currents iz, and iz. In this case, we demonstrate a illel connected ICCII+s as shown Fig.6. The perfected king in both magnitude and out of phase of iz, and iz, are wn in Fig.7(b) confirming a high precision property of this II+.

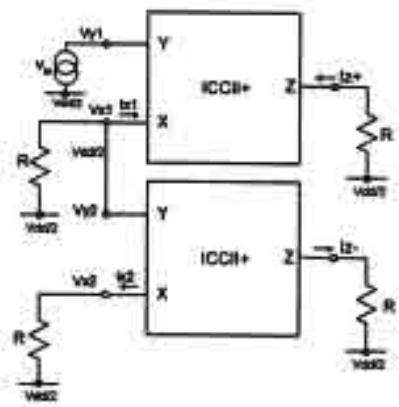


Fig.6 Parallel connected ICCII+s

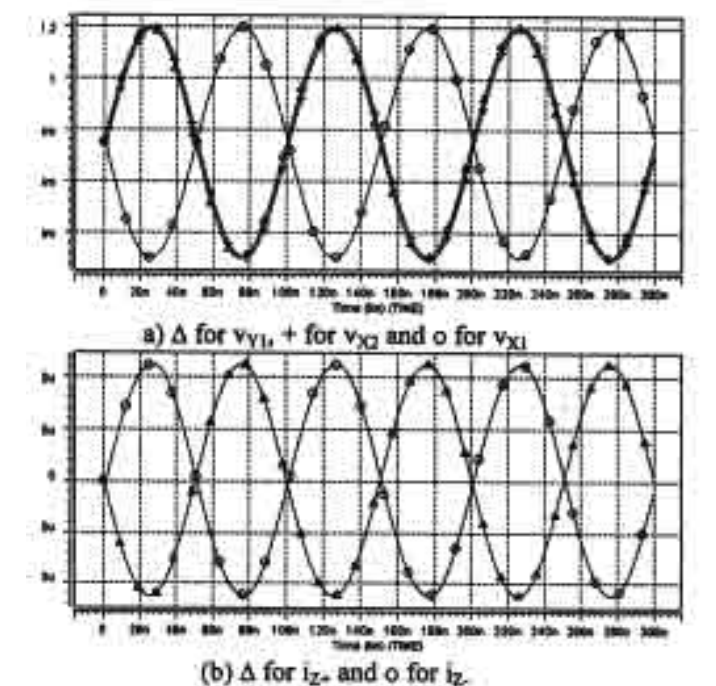


Fig.7 Transient responses at 10MHz with THD<1%

### IV. CONCLUSION

paper has presented a low voltage wide swing inverting nd generation CMOS current conveyor of which the gn focuses on the use of CMOS inverters and the negative

feedback to enhance conveying precisions, signal linearity and low output resistance property at the terminal X. The circuit is totally realized in class AB thanks to the use of CMOS inverters and the available floating-gate MOSFET additive analog inverter cell which facilitates the negative feedback channel to the normal CMOS inverter. With the programming approach of pseudo or quasi floating-gate MOSFET, DC offset of the floating-gate inverter can be effectively controlled to Vdd/2 and the complicated initial charge programming schemes could be avoided. The diode connected PMOSs producing the large resistors are always in reverse bias because the voltage at the floating-gate is small as a result of the negative feedback. With ±0.75V supply, the circuit can handle signal swing as large as ±500µA amplitude through X and Z terminals and ±500mV at Y and X terminals while the THD is maintained to less then 1%. The circuit is designed to operate up to 100MHz signal frequency.

### V. REFERENCES

 M.A. Ibrahim, H. Kuntman, "A CMOS realization of inverting second generation current conveyor", Proc. 2002, NORDIC Signal Processing Symposium, 2002.

[2] M.T. Abdelma Atti, N.A. Tasadduq, "New current-mode controlled filters using the controlled conveyor", Int. J. of Electronics, Vol.85, No.4, 1998, pp. 483-488.

[3] U. Yodprasit, "High-precision CMOS current conveyor", Electronics Letters, Vol. 36, No. 7, March 2000, pp.609-610.

[4] B. Maundy, I. Finvers, P. Aronhime, "A low voltage CMOS current conveyor for active filter design", Proc. MWSCAS-1998, August, 1998.

[5] A. J. Lopez-Martin, J. Ramirez-Angulo, R. G. Carvajal, "Low-voltage low-power wideband CMOS current conveyors based on the flipped voltage follower", Proc. ISCAS2003, pp.I-801-804.

[6] Y. Berg, O. Naess, M. Hovin, "Ultra low voltage floating-gate transconductance amplifier with tunable gain and linearity", Proc. ISCAS2000, pp. III-343-346.

[7] K. Moolpho, J. Ngammil, K. Nundhasri, "A low-voltage wideswing FGMOS current amplifier", Proc. ISCAS2002, May, 2002.

[8] T. Shibata, T. Ohmi, "A Functional MOS Transistor Featuring Gate-Level Weighted Sum and Threshold Operations", IEEE Trans. Elec. Devices, vol. 39, 1992, pp. 1444-1455.

[9] O. Naess, Espen A. Olsen, Y. Berg, T. S. Lande, "A low voltage second order biquad using pseudo floating-gate transistors", Proc. ISCAS2003, pp. 1-125-128.

[10] J. Ramirez-Angulo, A. J. Lopez-Martin, R. G. Carvajal, C. Lackey, "Low-voltage closed-loop amplifier circuits based on quasi-floating gate transistors", Proc. ISCAS2003, pp.I-813-816.

[11] J. Ramirez-Angulo, C. Urquidi, R. G. Carvajal, A.Torralba, "Sub-volt supply analog circuits based on quasi-floating gate transistors", Proc. ISCAS2003, pp.1-781-784.

[12] I.A. Awad, A.M. Soliman, "Inverting second generation current conveyors: the missing building blocks, CMOS realizations and applications", Int. J. Electronics, Vol. 86, pp.413-432, 1999.

Acknowledgement: This work has been supported by a grant from the Thailand Research Fund (TRF). Authors are grateful to the TRF for their precious support.

